Molecular Microbiology (2015) 95(3), 472–490 ■
doi:10.1111/mmi.12878
First published online 22 December 2014

The Rab GTPase YPT-1 associates with Golgi cisternae and Spitzenkörper microvesicles in *Neurospora crassa*

Eddy Sánchez-León,[1] Barry Bowman,[2] Constanze Seidel,[3†] Reinhard Fischer,[3] Peter Novick[4] and Meritxell Riquelme[1*]

[1]*Department of Microbiology, Center for Scientific Research and Higher Education of Ensenada (CICESE), Ensenada, Baja California, Mexico.*
[2]*Department of Molecular, Cell and Developmental Biology, University of California, Santa Cruz, CA, USA.*
[3]*Department of Applied Microbiology, Karlsruhe Institute of Technology, Karlsruhe, Germany.*
[4]*Department of Cellular and Molecular Medicine, University of California, San Diego, CA, USA.*

Summary

Vesicle traffic involves budding, transport, tethering and fusion of vesicles with acceptor membranes. GTP-bound small Rab GTPases interact with the membrane of vesicles, promoting their association with other factors before their subsequent fusion. Filamentous fungi contain at their hyphal apex the Spitzenkörper (Spk), a multivesicular structure to which vesicles concentrate before being redirected to specific cell sites. The regulatory mechanisms ensuring the directionality of the vesicles that travel to the Spk are still unknown. Hence, we analyzed YPT-1, the *Neurospora crassa* homologue of *Saccharomyces cerevisiae* Ypt1p (Rab1), which regulates different secretory pathway events. Laser scanning confocal microscopy revealed fluorescently tagged YPT-1 at the Spk and putative Golgi cisternae. Co-expression of YPT-1 and predicted post-Golgi Rab GTPases showed YPT-1 confined to the Spk microvesicular core, while SEC-4 (Rab8) and YPT-31 (Rab11) occupied the Spk macrovesicular peripheral layer, suggesting that trafficking and organization of macro and microvesicles at the Spk are regulated by distinct Rabs. Partial colocalization of YPT-1 with USO-1 (p115) and SEC-7 indicated the additional participation of YPT-1 at early and late Golgi trafficking steps.

Accepted 18 November, 2014. *For correspondence. E-mail riquelme@cicese.mx; Tel. +52 646 1750500 ext. 27051; Fax +52 646 1750595 ext. 27052. †Present address: Manchester Fungal Infection Group, Institute of Inflammation and Repair, University of Manchester, Manchester M13 9NT, UK.

Introduction

In eukaryotic cells, the transport of proteins through the distinct membranous compartments of the secretory pathway is carried out in vesicles. The fidelity of the vesicles delivered to the membrane domains of the acceptor compartments requires the coordinated action of GTPases of the Rab family, protein coats, molecular motors, SNARE proteins and tethering factors (Grosshans *et al.*, 2006). Rab proteins are highly conserved small GTPases that regulate vesicle traffic, and have the ability to oscillate between an inactive GDP-bound and an active GTP-bound state. The exchange of the bound GDP for GTP is catalyzed by Guanine nucleotide Exchange Factors (GEFs), while the hydrolysis of GTP to GDP is catalyzed by GTPase Activating Proteins (GAPs). The coordinated actions of GEFs and GAPs on specific Rab GTPases allow them to associate with membrane carriers, and to interact with specific effectors at the acceptor membranes in a regulated manner (Mizuno-Yamasaki *et al.*, 2012).

More than 60 Rabs have been identified in mammalian cells, and about 8 to 12 Ypts (Rab homologues) have been identified in fungi (Pereira-Leal and Seabra, 2000; Schultz *et al.*, 2000; Bourett *et al.*, 2007). In the secretory pathway, the regulation of the anterograde traffic of vesicles has been ascribed mainly to the activity of three Rabs: Rab1, Rab8 and Rab11. In *Saccharomyces cerevisiae*, Ypt1p, the orthologue of the mammalian Rab1, is involved in membrane traffic from the ER to early Golgi (Jedd *et al.*, 1997; Schultz *et al.*, 2000; Sacher *et al.*, 2001), intra-Golgi (Suvorova *et al.*, 2002) and from early endosomes to late Golgi (Du and Novick, 2001; Lafourcade *et al.*, 2004; Sclafani *et al.*, 2010). Ypt31p and Ypt32p are the functional homologues of the mammalian Rab11, involved in the budding of late Golgi vesicular carriers, a traffic event downstream of Ypt1p (Benli *et al.*, 1996; Jedd *et al.*, 1997). The final stages of the secretory pathway are regulated by the Rab8 orthologue, Sec4p, which has been localized at sites of polarized secretion (Salminen and Novick, 1987) and is implicated in tethering events at the plasma membrane, together with the exocyst complex subunit Sec15p (Guo *et al.*, 1999).

The Golgi apparatus is considered one of the most important sorting organelles for proteins in transit to the plasma membrane. Golgi morphology and organization in

the budding yeast and filamentous fungi differ significantly from the characteristic stacked cisternae described for animal and plant cells (Faso *et al*., 2009; Pantazopoulou and Peñalva, 2009; Lowe, 2011; Noda and Yoda, 2013). In filamentous fungi, the Golgi appears as individual smooth-surfaced cisternae, fenestrated hollow spheres or tubules (Girbardt, 1970; Grove and Bracker, 1970; Howard, 1981; Pantazopoulou and Peñalva, 2009). It has been suggested that the differences in Golgi organization could correspond in part to the membrane trafficking activity of the Golgi-associated Rab proteins (Liu and Storrie, 2012). Recently, in the filamentous fungus *Aspergillus nidulans*, alterations in the Golgi organization were linked to RabO, the Ypt1p orthologue (Pinar *et al*., 2013a). Even though it is widely known that Rab GTPases play significant roles in the anterograde and retrograde traffic of membranes within the secretory pathway in *S. cerevisiae* or mammalian cells, relatively little is known about their role in hyphal morphogenesis in filamentous fungi.

Fungal hyphae, neurons, root hairs and pollen tubes, all share the unique characteristic of growing at their tips, which results from the asymmetrical and continuous delivery of the necessary precursors for cell wall and membrane expansion (Heath, 1990; Geitmann and Emons, 2000). The origin of the vesicular carriers that transport enzymes responsible for the synthesis of the cell wall components in fungi is presently unclear (Riquelme *et al*., 2007; Verdín *et al*., 2009). Most hyphae contain at their apices a specialized multivesicular component, the Spitzenkörper (Spk), which is proposed to act as a Vesicle Supply Center, where cargo-carrying vesicles accumulate before being redirected to tip growing regions (Bartnicki-Garcia *et al*., 1989). Because of its composition and spatio-temporal localization, the Spk is considered a crucial player in hyphal apical growth and morphogenesis (Riquelme *et al*., 2011). Evidence from transmission electron microscopy has shown that the main constituents of the Spk are vesicles, actin filaments and ribosomes (Grove and Bracker, 1970; Howard, 1981; Roberson and Vargas, 1994). Two main regions can be defined at the Spk: the 'core' or inner region, mainly occupied by microvesicles (20–40 nm in diameter), and the outer region, occupied by macrovesicles (70–100 nm in diameter) (Bartnicki-Garcia, 1990; Riquelme and Sánchez-León, 2014). The microvesicles are indeed chitosomes, which carry chitin synthases (Riquelme *et al*., 2007; Sánchez-León *et al*., 2011). At the macrovesicular layer, subunits of the exocyst complex and enzymes necessary for β-(1, 3)-glucan synthase activity have been found (Verdín *et al*., 2009; Riquelme and Sánchez-León, 2014; Riquelme *et al*., 2014). Little is known about the biogenesis and transport of the cell wall-building vesicular carriers that constitute the Spk. Therefore, in this study we have investigated the intracellular distribution of the *Neurospora crassa* Rab GTPase YPT-1. Its localization at the Spk core and Golgi cisternae indicates that it participates both in late and early steps of the secretory pathway.

Results

N. crassa YPT-1, YPT-31 and SEC-4 localized at distinct layers of the Spk

A homologue of the small GTPase Ypt1p/Rab1 encoding gene had been previously identified in the *N. crassa* genome (Heintz *et al*., 1992; Borkovich *et al*., 2004). To characterize its subcellular distribution in *N. crassa*, YPT-1 was fluorescently tagged at its N-terminus and expressed under the control of the glucose repressible promoter *ccg-1* (P*ccg-1*) and the *ypt-1* gene promoter (P*ypt-1*). No differences were observed in the subcellular distribution of GFP-YPT-1 expressed under the control of the P*ccg-1* or the P*ypt-1* promoters (Fig. 1A, panels 1, 2). Western blots revealed similar expression levels of GFP-YPT-1 when expressed under control of the P*ccg-1* or the P*ypt-1* promoter (Fig. S1). In both cases, the *gfp*-tagged version of *ypt-1* was directed to the *his-3* site, and the selected strains contained the native copy of *ypt-1*. It was not possible to recover viable homokaryon *ypt-1Δ* strains (data not shown). Thus, the functionality of the GFP tagged YPT-1 was not tested. GFP-YPT-1 was observed at the Spk of all vegetative growing hyphae examined (Fig. 1A, panel 1, arrow). To confirm that YPT-1 was indeed confined to the core of the Spk we used the lipophilic dye FM4–64, which has been widely used to stain membranous structures such as the Spk (Fischer-Parton *et al*., 2000). FM4–64 stained primarily the outer layer of the Spk, surrounding the GFP-YPT-1 core (Fig. 1B, panel 1). We then further proceeded to analyze whether YPT-1 associates with a specific population of vesicles within the Spk. *N. crassa* chitosomes are usually observed at the microvesicular region of the Spk (Riquelme *et al*., 2007; Sánchez-León *et al*., 2011); therefore, we analyzed the distribution pattern of mChFP-YPT-1 and CHS-1-GFP at the Spk in a heterokaryon strain expressing both recombinant proteins. Co-expression revealed a conspicuous co-localization of both proteins at the Spk core (Fig. 1B, panel 2). Densitometry analysis of the Western blots of fractions obtained by sucrose density gradients (10–65%) showed that although GFP-YPT-1-associated structures (50 kDa bands) were present in all fractions (2–18) analyzed, the highest concentration of GFP-YPT-1 was found within the density range of 1.119–1.138 g ml^{-1} (fractions 10–12), characteristic of chitosomes (Fig. S2). The *N. crassa* β-(1, 3)-glucan synthase-related protein (GS-1) has been previously observed at the macrovesicular layer of the Spk (Verdín *et al*., 2009). The distribution of GS-1 at this layer of the Spk coincides with the distribution of macrovesicles observed

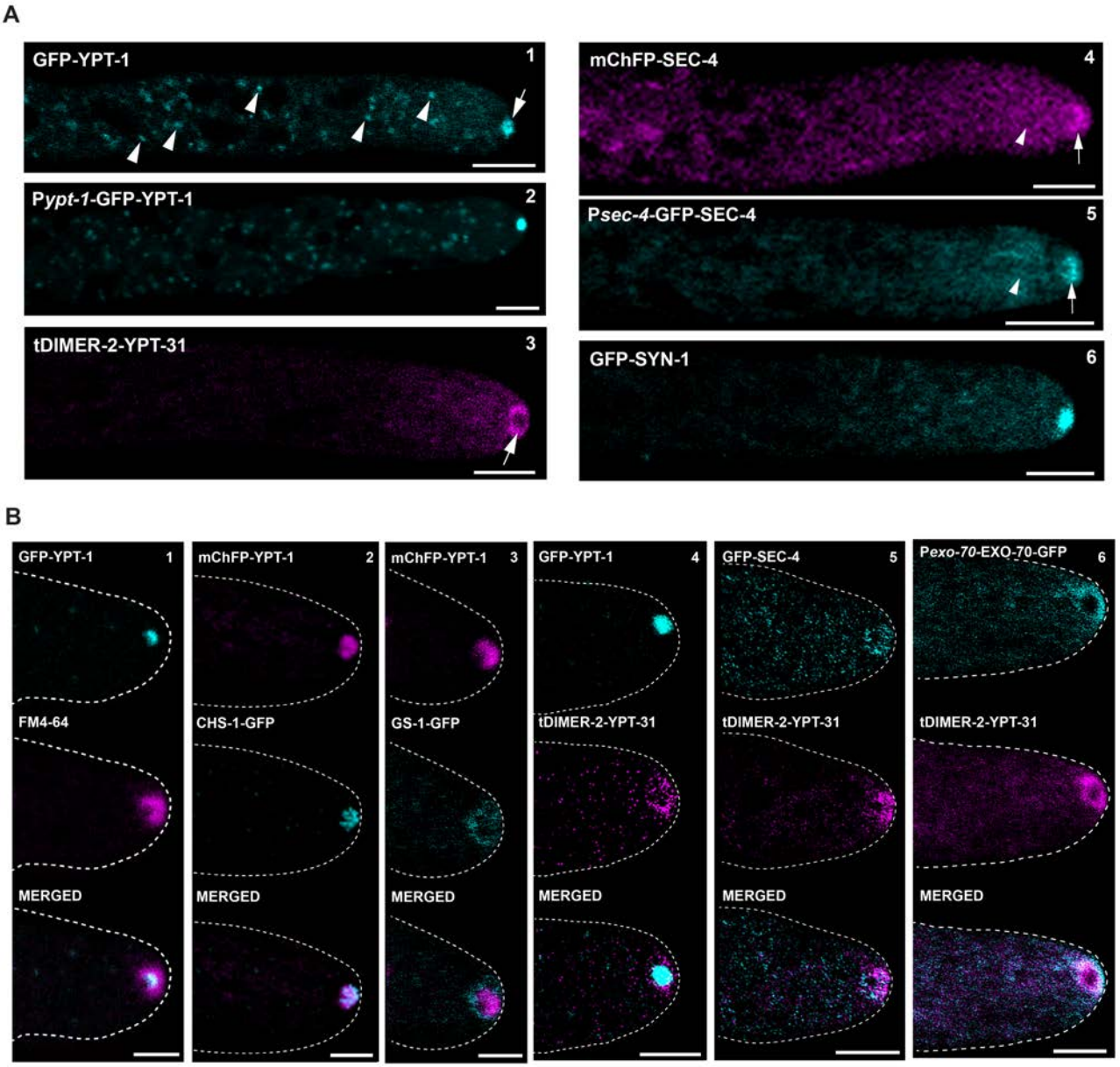

Fig. 1. Subcellular distribution of Rab GTPases YPT-1, YPT-31 and SEC-4 in *Neurospora crassa* growing hyphae.
A. LSCM analysis showed accumulation of YPT-1, YPT-31 and SEC-4 at distinct regions of the Spk (arrowheads). 1 and 2: GFP-YPT-1 expressed under the control of a copy of the endogenous promoter (P*ypt-1*) showed similar distribution patterns as observed in the strain expressing the heterologous protein under the control of the glucose repressible promoter P*ccg-1* (McNally and Free, 1988). At the apex, GFP-YPT-1 was observed at the Spk core, whereas at subapical and distal hyphal regions YPT-1 was observed at numerous punctate structures, presumably Golgi cisternae (arrowheads). 3–5: tDIMER-2-YPT-31 and SEC-4 were found at the Spk outer layer (arrowheads). No differences were found in the distribution patterns of SEC-4 expressed under the control of a copy of the corresponding endogenous promoter (P*sec-4*) or SEC-4 tagged with mChFP expressed under the P*ccg-1* promoter. SEC-4 also accumulated at the subapex behind the Spk (arrowhead). 6: GFP-SYN-1 was observed at the macrovesicular and microvesicular layers of the Spk. Bars, 5 μm.
B. 1: Rab GTPases YPT-1, YPT-31 and SEC-4 differentially associate with distinct vesicle populations of the Spk. Labeling with FM4–64 confirmed that GFP-YPT-1 was confined to the Spk core. 2: Co-expression of mChFP-YPT-1 and CHS-1-GFP, a GFP labeled chitin synthase previously found at the microvesicular core of the Spk (Sánchez-León *et al.*, 2011), showed clear co-localization of YPT-1 and CHS-1 at the Spk core. 3: Co-expression of mChFP-YPT-1 and GS-1-GFP, a GFP labeled glucan synthase-related protein identified previously at the macrovesicular layer of the Spk (Verdín *et al.*, 2009), indicated no co-localization of YPT-1 with the macrovesicular outer layer of the Spk. 4: YPT-31 was localized at the Spk outer layer surrounding the YPT-1 core. 5: The fluorescently tagged Rabs YPT-31 and SEC-4 were localized at the Spk outer layer. Note the variable labeling pattern of YPT-31 and SEC-4 at the outer vesicular layer of the Spk. 6: YPT-31 and the GFP tagged exocyst subunit EXO-70 (Riquelme and Sánchez-León, 2014; Riquelme *et al.*, 2014) showing partial co-localization at the Spk macrovesicular area. Bars, 2 μm.

by transmission electron microscopy of hyphal tips (Grove and Bracker, 1970; Howard, 1981). To further confirm that YPT-1 is excluded from the macrovesicular region of the Spk, we analyzed heterokaryon strains co-expressing GS-1-GFP and mChFP-YPT-1. It was clearly observed that mChFP-YPT-1 and GS-1-GFP occupied distinct layers of the Spk (Fig. 1B, panel 3).

In *S. cerevisiae* Rabs, Ypt31/32p associate with the late Golgi and newly formed post-Golgi carriers, where they participate in the recruitment of Sec2p, the GEF for Sec4p (Benli *et al*., 1996; Jedd *et al*., 1997; Ortiz *et al*., 2002). Sec4p participates downstream of Ypt31/32p at the last traffic events of the exocytic vesicles (Salminen and Novick, 1987; Goud *et al*., 1988). A previous analysis identified *N. crassa* YPT-31 (NCU01523) and SEC-4 (NCU06404) as the putative orthologues of the *S. cerevisiae* post-Golgi Rabs Ypt31/32p and Sec4p respectively (Borkovich *et al*., 2004). Blast search alignment of the *N. crassa* putative Rabs (SEC-4 and YPT-31) showed high overall identities (62–87%) at the amino acid level with their corresponding fungal and human orthologues (Table S2, Fig. S3). To determine whether YPT-31 and/or SEC-4 were involved in the traffic of vesicles that arrive at the Spk in *N. crassa*, we fluorescently tagged both Rabs at their N-terminus with the red fluorescent protein tDIMER-2 and GFP or mCherry, respectively, while maintaining their corresponding native copies. Confocal microscopy analysis of tDIMER-2-YPT-31 revealed its accumulation at the macrovesicular outer layer of the Spk (Fig. 1A, panel 3, arrow). Co-expression of tDIMER-2-YPT-31 with GFP-YPT-1 in a heterokaryon strain clearly confirmed the distribution of each protein in different layers of the Spk (Fig. 1B, panel 4). SEC-4 was mainly found at the outer macrovesicular region of the Spk (Fig. 1A, panel 4, arrow), but also some cytoplasmic fluorescence could be found at subapical hyphal regions (Fig. 1A, panel 4, arrowhead). Expression of the fluorescently tagged SEC-4 under the control of P*ccg-1* or the P*sec-4* promoters revealed no differences at the subcellular distribution (Fig. 1A, panels 4 and 5). Co-expression of tDIMER-2-YPT-31 and GFP-SEC-4, allowed the identification of both Rabs at the macrovesicular layer of the Spk, although the co-localization was only partial (Fig. 1B, panel 5). The distribution pattern of the Rabs YPT-31 and SEC-4 at the hyphal tips was variable due to the pleomorphic characteristics of the *N. crassa* Spk. To determine the accumulation of secretory vesicles at the Spk, the putative v-SNARE protein SYN-1 (NCU00566.7), used in other fungal species as vesicular marker (Lewis *et al*., 2000; Taheri-Talesh *et al*., 2008), was tagged with GFP at its N terminus. vSNAREs are members of the synaptobrevin protein family and are involved in fusion events of exocytic carriers during late steps of the secretory pathway (Protopopov *et al*., 1993; Grote *et al*., 2000; Shanks *et al*., 2012). A Blast search alignment revealed that *N. crassa* SYN-1 has a high identity level with the vSNAREs SynA of *A. nidulans* (64%; AN8769) and Snc2p of *S. cerevisiae* (58%; NP_014972). GFP-SYN-1 was observed at the macrovesicular and microvesicular layers of the Spk (Fig. 1A, panel 6; Fig. S4). In *N. crassa*, the components of the exocyst complex, EXO-70, EXO-84 and SEC-3, were found associated to the periphery of the Spk (Riquelme and Sánchez-León, 2014; Riquelme *et al*., 2014). We co-expressed tDIMER-2-YPT-31 and the previously GFP-tagged exocyst subunit EXO-70 (expressed under control of its own promoter), and observed partial co-localization of YPT-31 and EXO-70 at the Spk macrovesicular layer, although EXO-70 occupied primarily the area between the plasma membrane and YPT-31 labeled area (Fig. 1B, panel 6).

Vesicles flow into the Spk at very high rates

To determine the turnover rates of microvesicles and macrovesicles, we conducted fluorescence recovery after photobleaching (FRAP) analysis of GFP-YPT-1 or tDIMER-2-YPT-31. Photobleaching of the fluorescence at the Spk lasted 5 s. No fluorescence signal was detected at the Spk area immediately after photobleaching (Fig. 2A, panel 1–4, dotted circle at time 0.0 s). Fluorescence recovery of GFP-YPT-1, FM4–64, CHS-1-GFP, tDIMER-2-YPT-31 and GS-1-GFP occurred progressively at the Spk (Fig. 2A), where fluorescent spots appeared a few seconds after photobleaching (Fig. 2A, arrows). An increasing amount of GFP-YPT-1 or CHS-1-GFP over time was detected at the microvesicular/chitosomal core of the Spk, whereas the accumulation of FM4–64 occurred in the region surrounding the area occupied by GFP-YPT-1 (Fig. 2A, panels 1 and 2). Fluorescence recovery of tDIMER-2-YPT-31 and GS-1 occurred also progressively, but restricted to the macrovesicular layer of the Spk (Fig. 2A, panels 3 and 4). Half-time recovery values ($t_{1/2}$, Mean ± Standard Error), i. e. the time at which half of the final fluorescence intensity was reached, were assessed from the normalized fluorescence recovery values for GFP-YPT-1, FM4–64, tDIMER-2-YPT-31, CHS-1-GFP and GS-1-GFP (Fig. 2B). The $t_{1/2}$ was 15.5 ± 4.3 s ($n = 11$) for GFP-YPT-1, 21.3 ± 5.7 s ($n = 11$) for FM4–64, 21.5 ± 3.7 s ($n = 9$) for CHS-1-GFP and 9.9 ± 2.6 s ($n = 9$) for tDIMER-2-YPT-31 and 10.2 ± 1.7 s ($n = 12$) for GS-1-GFP. The one-way analysis of variance (ANOVA) post hoc Tukey-HSD test revealed significant differences between the $t_{1/2}$ of tDIMER-2-YPT-31 and GS-1-GFP compared with the $t_{1/2}$ of CHS-1-GFP and FM4–64, whereas no significant differences were found between the $t_{1/2}$ of GFP-YPT-1 and the rest of $t_{1/2}$ analyzed.

Total internal reflection fluorescence microscopy (TIRFM) analysis confirmed the conspicuous localization

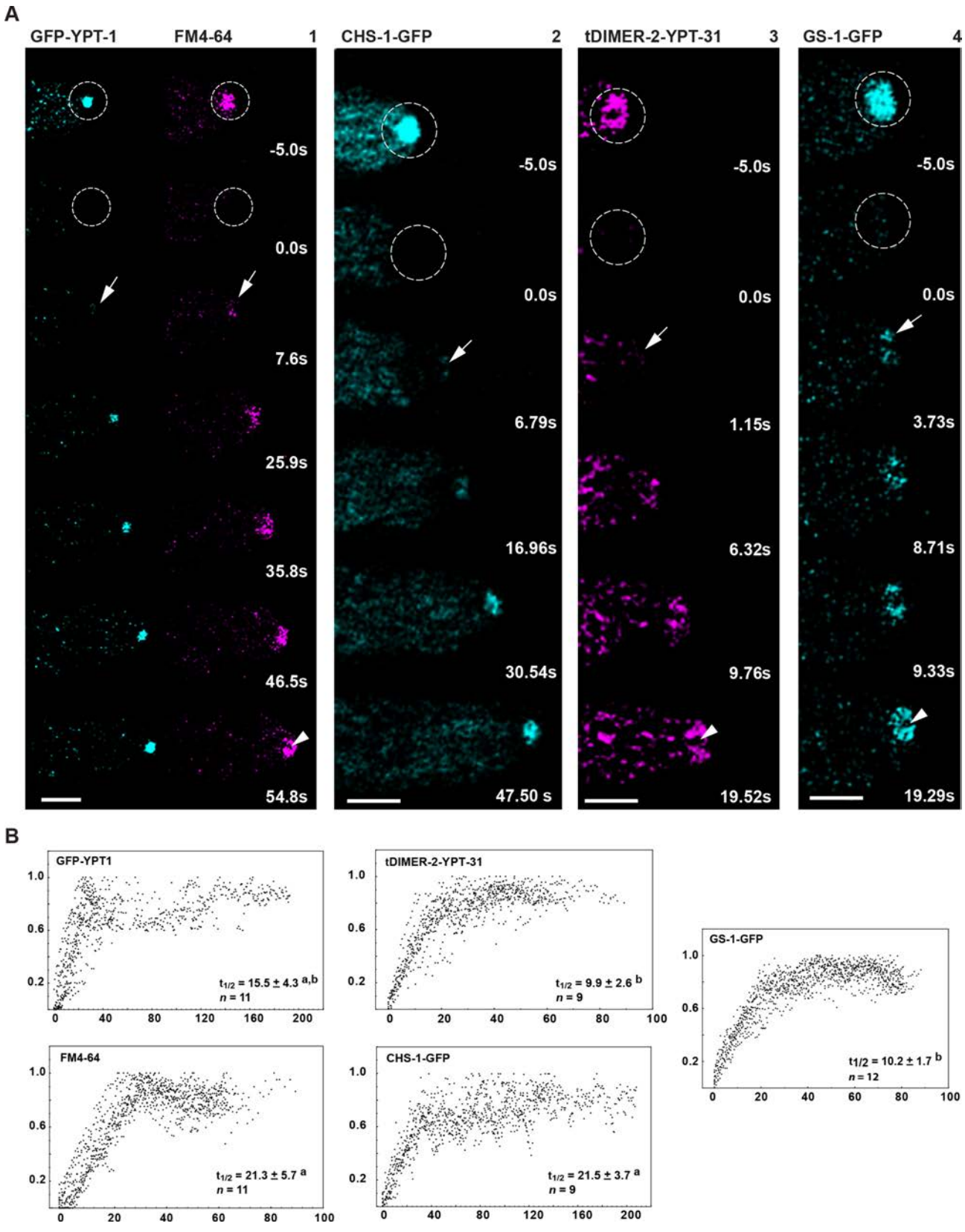
A
GFP-YPT-1
FM4-64
1
CHS-1-GFP
2
tDIMER-2-YPT-31
3
GS-1-GFP
4
-5.0s
0.0s
7.6s
25.9s
35.8s
46.5s
54.8s
-5.0s
0.0s
6.79s
16.96s
30.54s
47.50 s
-5.0s
0.0s
1.15s
6.32s
9.76s
19.52s
-5.0s
0.0s
3.73s
8.71s
9.33s
19.29s
B
GFP-YPT1
t1/2 = 15.5 ± 4.3 a,b
n = 11
tDIMER-2-YPT-31
t1/2 = 9.9 ± 2.6 b
n = 9
GS-1-GFP
t1/2 = 10.2 ± 1.7 b
n = 12
FM4-64
t1/2 = 21.3 ± 5.7 a
n = 11
CHS-1-GFP
t1/2 = 21.5 ± 3.7 a
n = 9

Fig. 2. FRAP analysis of Rab GTPases YPT-1 and YPT-31 at the Spk.
A. Photobleaching was performed for 5 s at the indicated hyphal tip region (dotted circle) before resuming image capturing. 1–4: FRAP of hyphal tips of *N. crassa* strains expressing: GFP-YPT-1 stained with FM4–64, the Spk microvesicular marker CHS-1-GFP, tDIMER-2-YPT-31 and the Spk macrovesicular marker GS-1-GFP. Fluorescent spots accumulated gradually over time at the Spk, while GFP-YPT-1 and CHS-1-GFP fluorescence occupied the Spk core FM4–64, tDIMER-2-YPT-31 and GS-1-GFP accumulated at the outer layer of the Spk (arrows). Note the Spk core lacking at the FM4–64, YPT-31 and GS-1 expressing strains (arrowheads). Bars, 5 μm.
B. Graphs show normalized fluorescence intensity recovery value plots and the half-time recovery values ($t_{1/2}$ = seconds; Mean ± Standard Error) of hyphae expressing GFP-YPT-1, CHS-1-GFP, tDIMER-2-YPT-31, GS-1-GFP and hyphae stained with FM4–64. Values bearing the same letter (i.e., a or b) are not significantly different by post hoc Tukey HSD test ($P = 0.00011$). Abscissas and ordinates show time in seconds and normalized fluorescence recovery values respectively.

of mChFP-YPT-1 at vesicles (Fig. 3A and B, arrowheads) and putative Golgi cisternae (Fig. 3A and B, arrows) moving fast and slow respectively. Kymographs confirmed not only variable speeds of the YPT-1 labeled structures (Fig. 3C, panel 1), but also that the movements were primarily parallel to the axis of hyphal growth (Fig. 3C, panel 2). Traces obtained from the kymographs revealed vesicles with fast (0.4–4 μm s^{-1}, $n > 50$) anterograde and retrograde movements (Fig. 3C, panels 3 and 4), which contrasted with the slow (< 0.5 μm s^{-1}, $n > 20$) anterograde motion recorded for the putative Golgi cisternae (Fig. 3C, panel 5).

YPT-1 associates with diverse subpopulations of Golgi cisternae

In addition to the Spk localization, GFP-YPT-1 was also observed as numerous fluorescent punctate structures along the cell (Fig. 1A, panel 1, arrowheads), which were distributed mainly at subapical and distal hyphal regions (8–49 μm from the tip, $n = 28$), although some labeled particles were observed at the proximal subapical hyphal regions near the tip (7 μm from the tip, $n = 28$). To determine if the GFP-YPT-1 punctate structures corresponded to Golgi cisternae, we examined the effects of brefeldin A

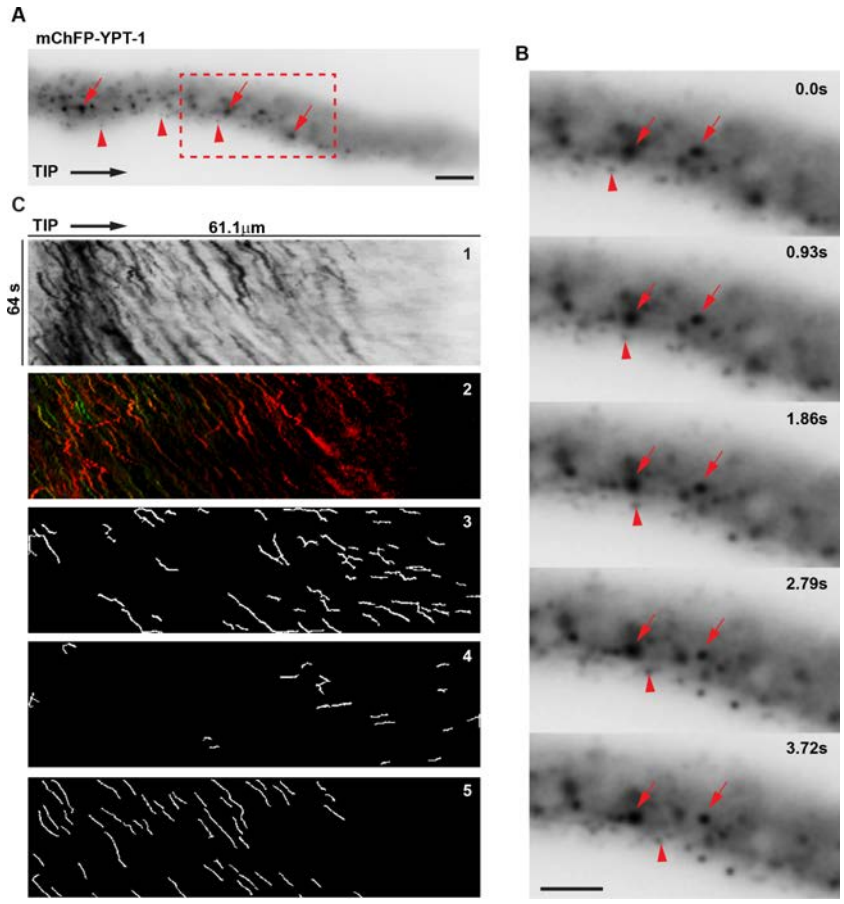

Fig. 3. Analysis of the dynamics of mChFP-YPT-1 associated structures.
A. TIRFM revealed mChFP-YPT-1 conspicuously localized at vesicles (arrowheads) and putative Golgi cisternae (arrows).
B. Time series showing the positional changes of a mChFP-YPT-1-associated vesicle in A (red dotted box). Note the considerable movement of a vesicle (arrowhead) in contrast with the slight movement of the Golgi cisternae (arrows).
C. 1: Kymograph of the hyphal section in A showing the spatio-temporal relation of mChFP-YPT-1 containing structures. 2: Color-Kymograph as in B showing the position of the mChFP-YPT-1 labeled structures perpendicular to the long axis of the hyphae. The green, yellow and red colors represent mChFP-YPT-1 labeled vesicles and Golgi cisternae at the top, middle or bottom sections of the hyphae respectively. Note the low cases of YPT-1 associated structures showing positional changes perpendicular to the long axis. Parts 3 and 4 show kymograph traces (0.4–4 μm s^{-1}) of mChFP-YPT-1 labeled vesicles, of the hyphal section in A, with anterograde and retrograde movement respectively. 5: Kymograph traces (< 0.5 μm s^{-1}) of Golgi cisternae with anterograde movement. Bars, 5 μm.

(BFA) on the intracellular distribution of GFP-YPT-1. The addition of BFA to growing hyphae induced the formation of GFP-YPT-1 clusters and a reduction of putative Golgi punctate structures (Fig. 4A, Movie S1). When exposed to BFA, accumulation of GFP-YPT-1, tDIMER-2-YPT-31 and GFP-SEC-4 at the hyphal apex was temporarily interrupted, concomitant with a temporary cessation of apical growth, tips swelling and Spk disassembly of the Rabs (Fig. 4A). BFA treatment of hyphae co-expressing CHS-1-mChFP or tDIMER-2-YPT-31 and GFP-YPT-1 showed clustering of the YPT-1 punctate structures, but no accumulation of CHS-1 or YPT-31 at any of these structures (Fig. S5, Movie S1). Interestingly, during BFA exposure we observed CHS-1-mChFP, but not GFP-YPT-1 at the Spk. To further analyze the *N. crassa* YPT-1 distribution at the distinct subpopulations of Golgi cisternae, we co-expressed GFP- or mChFP-YPT-1 with different Golgi markers such as USO-1, VRG-4, VPS-52 and SEC-7, and exposed the cells to BFA. In *S. cerevisiae* and mammals, Uso1p/p115 is a long coil-coiled tethering protein, which is recruited by Ypt1p/Rab1 (Cao *et al*., 1998; Allan *et al*., 2000) and is necessary, through the interaction with GM130 (Barr *et al*., 1998; Shorter and Warren, 1999; Moyer *et al*., 2001) for the tethering of ER-derived membrane carriers to early Golgi membranes (Beard *et al*., 2005). The expression of USO-1-GFP under the control of its own promoter showed numerous fluorescent punctate structures distributed along the hyphae (Fig. 4B). The morphology and subcellular distribution of the USO-1-GFP labeled structures resembled that of the putative Golgi cisternae marked by YPT-1 (Fig. 1A, panel 1). At distal and subapical distal hyphal regions (> 36.2 µm from the tip, $n = 30$), USO-1-GFP and mChFP-YPT-1 co-localized at numerous particles, presumably early Golgi cisternae (Fig. 4C, panel 1, arrowheads; Fig. 4D). Although both proteins co-localized at some structures, the pattern of the fluorescence signal exhibited pleomorphisms (Fig. 4C, panel 1, 3–6; Movie S2), which might result from the dynamic behavior of the Golgi cisternae during maturation. Numerous mChFP-YPT-1 structures that did not co-localize with USO-1-GFP were also observed along different hyphal regions (Fig. 4C, arrows). After BFA exposure, a change in the distribution of fluorescent cisternae was clearly observed (Fig. 4C, panel 2). Visual inspection of the fluorescent signals suggested that almost all USO-1-GFP labeled cisternae co-localized with a fraction of the mChFP-YPT-1 labeled cisternae (Fig. 4C, panel 2, bottom image). To verify the extent of co-localization, the Intensity Correlation Quotient (ICQ) was calculated from the images corresponding to hyphae treated with BFA and untreated. The ICQ index measures the relationship of the relative intensities of two fluorescent particles (Li *et al*., 2004). A random distribution of two fluorescent particles has an ICQ value around 0, while co-localizing and nonco-localizing particles have ICQ values within the range of $0 < \text{ICQ} \leq +0.5$ and $0 > \text{ICQ} \geq -0.5$ respectively. In untreated cells, ICQ values (Mean ± Standard Error) were 0.144 ± 0.026 ($n = 8$), whereas in BFA-treated cells ICQ values were significantly higher, 0.212 ± 0.019 ($n = 5$) (Student's *t*-test, $P < 0.01$).

The Vrg4 protein is a mannose transporter, whose localization has been reported at Golgi structures in different fungal systems (Dean *et al*., 1997; Nishikawa *et al*., 2002; Jackson-Hayes *et al*., 2008; Bowman *et al*., 2012). Experimental evidence on the GDP-mannose transporter of *S. cerevisiae*, Vrg4p, suggests that the protein recycles between ER and Golgi (Abe *et al*., 2004). To further analyze the distribution of YPT-1 at the different Golgi cisternae populations, we co-expressed mChFP-YPT-1 and VRG-4-GFP. Image analysis revealed co-localization of VRG-4-GFP and mChFP-YPT-1 in a subpopulation of Golgi cisternae (Fig. 4E, panel 1, arrowheads; Movie S3). Although co-localizing structures were present, numerous single labeled structures were observed (Fig. 4E, panel 1, arrows). BFA exposure induced the typical clustering of mChFP-YPT-1 labeled cisternae, which co-localized with all the VRG-4-GFP labeled cisternae (Fig. 4E, panel 2, arrowheads). The ICQ value increased from 0.091 ± 0.025 ($n = 12$) in untreated cells to 0.201 ± 0.025 ($n = 10$), significantly higher (Student's *t*-test, $P < 0.01$), in BFA-treated cells.

To determine if the YPT-1 single labeled structures observed in the above experiments corresponded to late Golgi cisternae, co-localization analyses were performed with the *N. crassa* putative orthologue of Sec7p and YPT-1. In *S. cerevisiae*, *SEC7* encodes a guanine-nucleotide exchange factor, which activates Arf GTPases at the late (*trans*-) Golgi cisternae (Achstetter *et al*., 1988; Sata *et al*., 1998). An analysis of the intracellular localization and dynamics of Golgi in *S. cerevisiae* and *A. nidulans* revealed that Sec7 could be used as a bona fide marker of late Golgi cisternae (Losev *et al*., 2006; Matsuura-Tokita *et al*., 2006; Pantazopoulou and Peñalva, 2009). Blast search alignment revealed that the *N. crassa* NCU07658.7 encodes a protein with an overall identity of 38% and 57% with the *S. cerevisiae* Sec7p (NP_010454) and *A. nidulans* $\text{HypB}^{\text{Sec7}}$ (AN6709) proteins respectively. Additionally, the predicted amino acid sequence has the Sec7 domain (Pfam: PF01369). Therefore, the *N. crassa* NCU07658.7 was designated as SEC-7. The endogenously GFP tagged SEC-7 was identified at several fluorescent punctate structures, presumably late Golgi cisternae, distributed along the cells (Fig. 5A, $n > 30$); occasionally, some of these structures were observed near hyphal tips (Fig. 5A, arrowheads). As predicted, the co-expression of SEC-7-GFP and mChFP-YPT-1 revealed that both proteins co-localized at some of the putative late Golgi cisternae (Fig. 5B, panel 1). This co-localization increased slightly

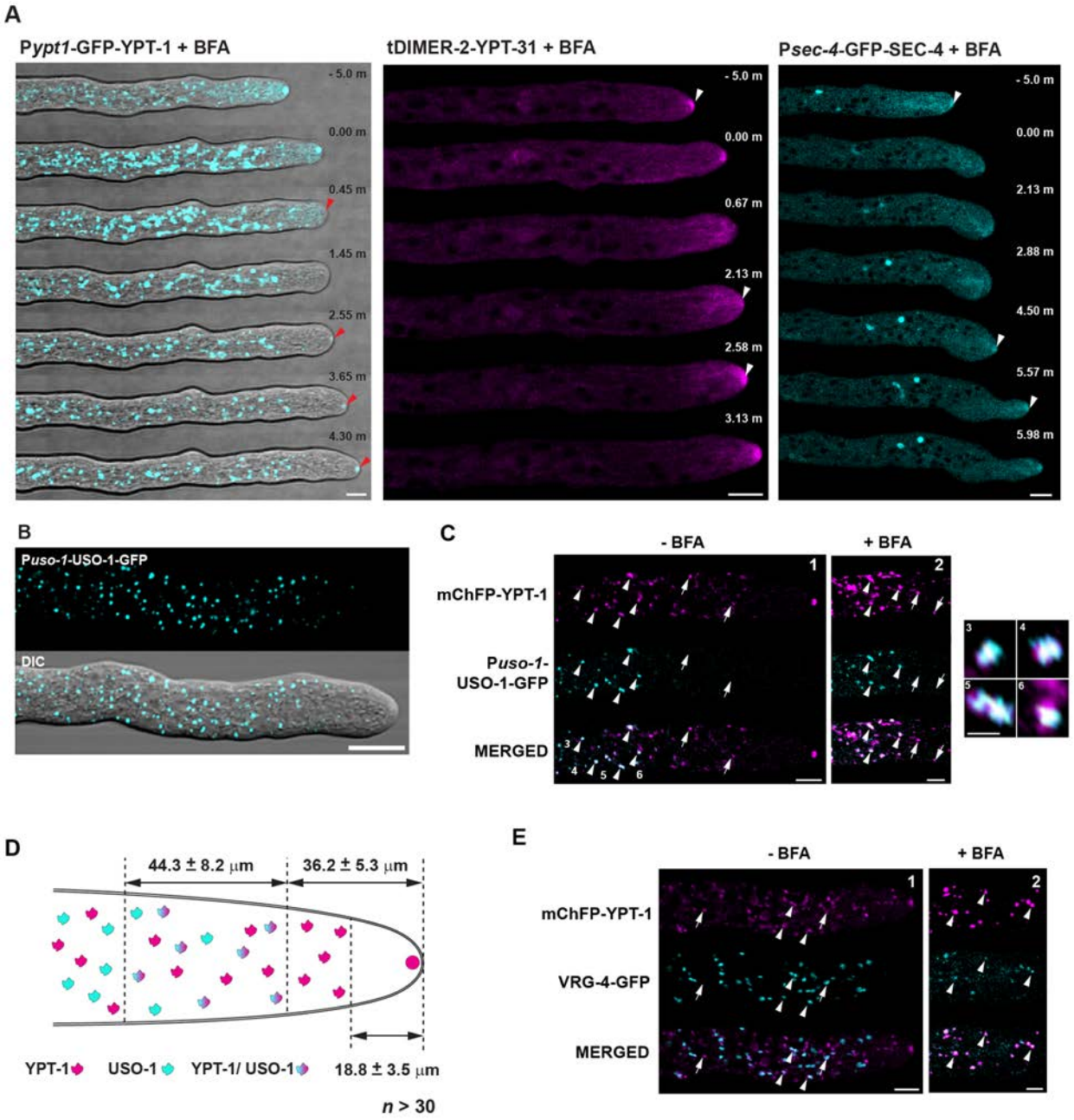

Fig. 4. YPT-1 associates with different subpopulations of Golgi cisternae.
A. BFA treatment in cells expressing the fluorescently tagged YPT-1, YPT-31 and SEC-4 did not cause any clustering of tDIMER-2-YPT-31 or GFP-SEC-4 as observed for GFP-YPT-1. The Spk localization of the Rabs was temporarily interrupted while the hyphae experienced tip swelling. Bars, 5 µm.
B. LSCM analysis showed USO-1-GFP at numerous punctate structures distributed at the proximal and distal subapical hyphal regions. Bars, 5 µm.
C. 1: Co-expression of mChFP-YPT-1 and the early Golgi marker USO-1-GFP (arrowheads) showed co-localization of YPT-1 and USO-1 at some of the Golgi cisternae located at distal and subapical distal regions of the cells. 2: BFA exposure caused the aggregation of USO-1-GFP and mChFP-YPT-1 (arrowheads). Note that a small fraction of mChFP-YPT-1 clusters (arrows) did not co-localize with USO-1-GFP. 3–6: Digital magnification of co-localizing particles in panel 1 (arrowheads) shows both proteins occupying distinct domains within the identified Golgi cisternae. Bars, 5 µm.
D. Illustration of the subcellular distribution of cisternae containing mChFP-YPT-1 and USO-1-GFP and their positions from the tip (Mean ± Standard Error).
E. 1: Co-expression of mChFP-YPT-1 and VRG-4-GFP (Bowman *et al.*, 2012) showed a mixed population of co-localizing (arrowheads) and single (arrows) labeled cisternae. 2: mChFP-YPT-1 clusters resulting from the BFA exposure co-localized with VRG-4-GFP containing cisternae (arrowheads). Bars, 5 µm.

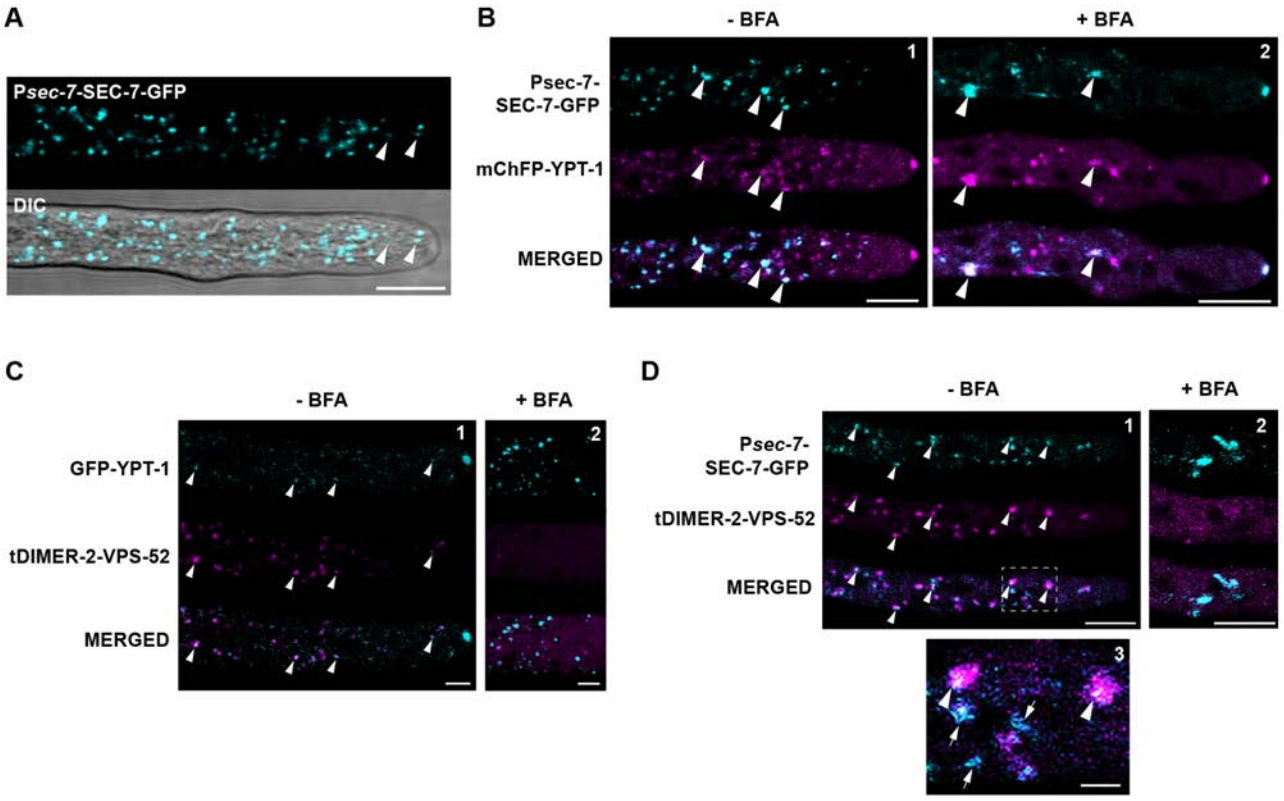

Fig. 5. YPT-1 distribution at late Golgi cisternae.
A. LSCM analysis of the GFP-tagged version the late Golgi marker SEC-7 was observed at numerous punctate structures distributed at subapical and distal hyphal regions. Note the presence of SEC-7-GFP at the hyphal apex. Bar, 10 μm.
B. 1: Co-expression of mChFP-YPT-1 and SEC-7-GFP showed partial co-localization at the observed late Golgi cisternae (arrowheads). 2: BFA exposure caused the reduction and clustering of the YPT-1 and SEC-7 fluorescent structures, showing also some co-localization (arrowheads). Note the presence of GFP-SEC-7 at the Spk. Bars, 10 μm.
C. 1: Co-expression of GFP-YPT-1 and tDIMER-2-VPS-52 (Bowman *et al.*, 2012) showed that all VPS-52 particles co-localized (arrowheads) with a subpopulation of YPT-1 cisternae. 2: BFA exposure caused the loss of RFP-VPS-52 at any of the GFP-YPT-1 containing cisternae. Bars, 5 μm.
D. 1: SEC-7-GFP and tDIMER-2-VPS-52 were identified at numerous punctate structures which displayed partial co-localization (arrowheads). 2: Clustering of SEC-7 and disassembly of VPS-52 under the effect of BFA. Bars, 10 μm. 3: Digital magnification of the fluorescent particles in panel 1 showing both proteins at the same structures (arrowheads) but also at isolated punctate (arrows). Bar, 2 μm.

after BFA treatment (Fig. 5B, panel 2). ICQ values before and after BFA treatment were 0.122 ± 0.037 ($n = 5$) and 0.154 ± 0.030 ($n = 8$) respectively. Unexpectedly, BFA treatment promoted the accumulation of SEC-7-GFP at the Spk (Fig. 5B, panel 2; $n > 20$), in contrast to the untreated cells.

To further analyze whether the YPT-1 labeled structures corresponded to late Golgi compartments, intracellular distribution of YPT-1 and the GARP complex subunit VPS-52 was analyzed. The GARP (Golgi-associated retrograde protein) complex is a multimeric tethering factor involved in the retrograde traffic of endosome-derived carriers to late Golgi or TGN (Conibear and Stevens, 2000). The GARP complex, composed of VPS-51p, -52p, -53p and -54p, is recruited by Ypt6p/Rab6 to the late Golgi (Siniossoglou and Pelham, 2001; Liewen *et al.*, 2005). In *A. nidulans*, the yeast Ypt6p homologue, RabC^{Rab6}, was identified at early and late Golgi compartments (Pantazopoulou and Peñalva, 2011). In previous studies, localization analysis in *N. crassa* identified the fluorescently tagged VPS-52 at Golgi cisternae mainly separated from the early Golgi cisternae labeled by the calcium transporter PMR-1, which lead the authors to suggest that VPS-52 localizes at late Golgi cisternae (Bowman *et al.*, 2012). Previous studies in *S. cerevisiae* found Ypt1p at late Golgi cisternae, and reported that this Rab GTPase regulates the traffic of vesicles at the early endosome-late Golgi interface (Sclafani *et al.*, 2010). To determine if a subpopulation of Golgi cisternae labeled with YPT-1 corresponded to late Golgi cisternae, we co-expressed tDIMER-2-VPS-52 and GFP-YPT-1. As predicted, some of the tDIMER-2-VPS-52 containing Golgi cisternae coincided with GFP-YPT-1 Golgi cisternae (Fig. 5C, panel 1, arrowheads). Image analysis yielded an ICQ of 0.177 ± 0.013 ($n = 4$). Under the effects of BFA, tDIMER-2-VPS-52 was dispersed into the cytosol (there was an increase in the red

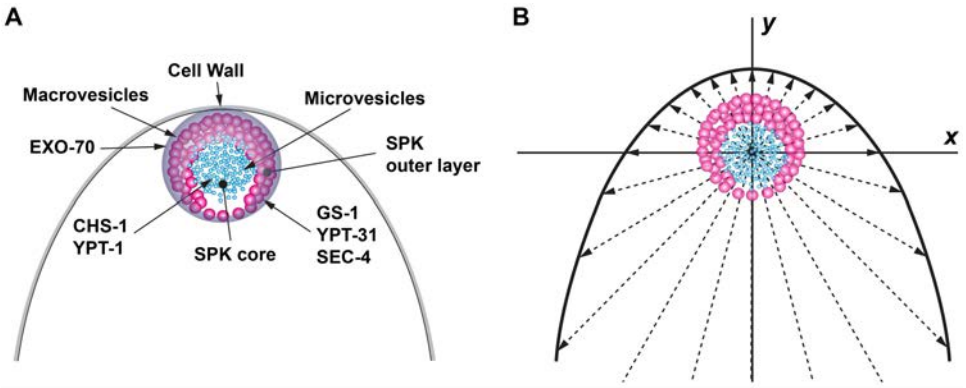

Fig. 6. Rab GTPases distribution at the Spk.
A. Schematic representation of the distribution of Rab proteins at the different Spk layers where various markers have been previously found.
B. Illustration overlaying the stratified accumulation of micro and macrovesicles found at the Spk of *N. crassa* and the VSC model for hyphal morphogenesis (Bartnicki-Garcia *et al.*, 1989). According to the model, the VSC (= Spk) collects vesicles arriving from distal parts of the hypha and distributes them in all directions until they reach and fuse with the plasma membrane.

fluorescence signal of the cytoplasm) and was no longer observed in the putative late Golgi cisternae (Fig. 5C, panel 2). Co-expression of SEC-7-GFP and tDIMER-2-VPS-52 showed both proteins partially co-localizing at the same structures (Fig. 5D, panel 1 and 3). Co-localization analysis yielded an ICQ of 0.113 ± 0.017 ($n = 21$). BFA treatment induced the aggregation of SEC-7-GFP marked Golgi and the dispersion of tDIMER-2-VPS-52 to the cytosol (Fig. 5D, panel 2).

YPT-1 distributes along a tubular network

In addition to the identification of YPT-1 at Golgi cisternae, and at the core of the Spk (see results above), we found YPT-1 at other subcellular membranes. At distal hyphal regions (79.6 ± 22.8 μm, $n = 7$), mChFP-YPT-1 was found decorating numerous tubule-like structures (Fig. S6A, panel 1). None of these tubular structures were observed near the distal subapical or apical regions of the hyphae. TIRFM analysis showed that the length and position of the YPT-1 tubules varied along the hyphae (Fig. S6B). The tubular structures frequently arranged into a loose network of filaments that displayed a very dynamic behavior (Fig. S6C; Movie S4); sometimes, they were found forming branches and loops (Fig. S6C). To examine the possibility that the YPT-1 tubules corresponded to microtubules, we co-expressed mChFP-YPT-1 and the GFP tagged β-tubulin (BML-GFP). No co-localization of any of the structures was found, confirming that the YPT-1 tubule-like structures are not associated with microtubules (Fig. S6A, panel 2–4; Movie S5).

YPT-1 does not localize at early endosomes

Previous studies have shown that Rab1/Ypt1p has a role in endocytic traffic (Sclafani *et al.*, 2010; Mukhopadhyay *et al.*, 2011). While several of our observations indicated that YPT-1 localized primarily at the different Golgi cisternae, we could not exclude the possibility that some of the GFP- or mChFP-YPT-1 labeled structures corresponded to early endosomes. Moreover, partial co-localization was observed between very few of the GFP-YPT-1 cytoplasmic punctate fluorescent structures and FM4–64 stained structures (Fig. S7A). To discern this, we co-expressed mChFP-YPT-1 with the previously GFP-tagged YPT-52, the *N. crassa* early endosome Rab5 homologue (Seidel *et al.*, 2013). None of the GFP-YPT-52 labeled endosomes co-localized with mChFP-YPT-1 (Fig. S7B; Movie S6). Each of the samples analyzed ($n = 8$) showed ICQ values of –0.5.

Discussion

The Spk is a pleomorphic structure implicated in the hyphal growth and morphogenesis of numerous fungal species (Riquelme and Sánchez-León, 2014). Previous studies have revealed that the conspicuous Spk of *N. crassa* hyphae contains a high concentration of vesicles of different sizes organized in different layers, and more importantly, that each type of vesicle contains cell wall-building enzymes of different nature (Riquelme *et al.*, 2007; Verdín *et al.*, 2009). Previously, RabC and RabO, the proteins in *A. nidulans* homologous to Rab6 and Rab1, respectively, were observed at the Spk (Pantazopoulou and Peñalva, 2011; Pinar *et al.*, 2013a). In this study, we identified the Rab proteins YPT-1, YPT-31 and SEC-4 at different layers of the Spk of *N. crassa* (Fig. 6A), suggesting that distinct Rabs might differentially regulate the traffic of the different populations of vesicles of the Spk. Fluorescent tagging of some Rab GTPases in other model systems has resulted in hypomorphic effects due to alterations in function and/or

stability of the tagged proteins (Pantazopoulou *et al*., 2014). We expressed fluorescently tagged versions of YPT-1, SEC-4 and YPT-31, while maintaining their corresponding native copies, resulting in strains with no growth defects (data not shown).

The steady fluorescence at the Spk suggests that the rate of discharge of vesicles from the Spk equals the rate of arrival of the vesicles to the Spk, consistent with the vesicle supply center (VSC) model for fungal morphogenesis, which proposed that secretory vesicles arriving from distal regions of the hyphae accumulate temporarily at the Spk prior to being discharged to the apical plasma membrane (Bartnicki-Garcia *et al*., 1989) (Fig. 6B). The turnover rates obtained from analysis of FRAP experiments indicated that the putative secretory vesicles exhibit a highly dynamic behavior at the Spk (Jones and Sudbery, 2010; Dijksterhuis and Molenaar, 2013; Pantazopoulou *et al*., 2014). FRAP analysis in *N. crassa* revealed a half-time recovery ($t_{1/2}$) for YPT-1 and YPT-31 between 10 and 16 s, suggesting the existence of high flow rates for vesicles reaching the Spk. In *A. nidulans* and *C. albicans*, a $t_{1/2}$ of 7 s and 10 s was obtained in FRAP experiments for the YPT-31 orthologue, $RabE^{RAB11}$ and Sec4 respectively (Jones and Sudbery, 2010; Pantazopoulou *et al*., 2014). In spite of the differences in growth rates reported for hyphae of *N. crassa* (~ 60 μm min^{-1}) (Hickey *et al*., 2002), *C. albicans* (0.25 μm min^{-1}) (Jones and Sudbery, 2010) and *A. nidulans* (0.5–1 μm min^{-1}) (Horio and Oakley, 2005), similar $t_{1/2}$ values were obtained for the above-mentioned Rabs, indicating that the rate of arrival of secretory carriers to the Spk is independent of hyphal growth rate. The $t_{1/2}$ values obtained for YPT-1 and YPT-31 were lower than those for FM4–64 and CHS-1, which could be indicative of the transient association of the Rabs with the secretory carriers, in contrast with CHS-1 and FM4–64, which are presumably embedded in the plasma membrane of the carriers. These results hint at the existence of a mechanism coordinated by Rabs that regulates the ordered delivery of vesicles to the Spk and their subsequent discharge to the apical cell surface.

We identified the *N. crassa* YPT-1 at the core of the Spk, co-localizing almost fully with CHS-1 (Fig. 6A). In a recent study, we have identified YPT-1 among the proteins that co-immunoprecipitated with CHS-1, CHS-4 and CHS-5 (Fajardo-Somera, unpublished). In addition, we found that GFP-YPT-1 sedimented in fractions with a density range similar to the density (1.125 g ml^{-1}) of the fractions with high chitin synthase activity reported previously (Bartnicki-Garcia *et al*., 1984; Leal-Morales *et al*., 1994; Verdín *et al*., 2009). Altogether, the evidence suggests that YPT-1 might have a role in the pre-exocytic traffic of microvesicles, including chitosomes. The putative role of YPT-1 in regulating vesicle traffic at the Spk, adds yet another role for Ypt1, other than the role described in *S. cerevisiae* and mammalian cells at the ER-Golgi interface, endosome-Golgi and autophagosome formation (Barrowman *et al*., 2010; Lynch-Day *et al*., 2010). This functional 'promiscuity' of Ypt1 at different steps of the secretory pathway must be precisely regulated by corresponding GEFs and GAPs.

Ypt31/32p have been localized at sites of polar growth in yeast (Jedd *et al*., 1997). They participate in a cascade mechanism, where they recruit to the membrane of secretory carriers Sec2p, a GEF that subsequently activates Sec4p (Ortiz *et al*., 2002). An analysis of the amino acid sequence of *N. crassa* Rab GTPases SEC-4 and YPT-31 revealed a high level of identity with Sec4p/Rab8 and Ypt32p/Rab11 respectively. In addition, sequence alignments showed a remarkable level of sequence conservation at the identified regions (G motifs, Switch Regions I and II, and RabSF1–4). Together, these results suggest that SEC-4 and YPT-31 of *N. crassa* are indeed homologous proteins of Rab8 and Rab11 respectively. In *N. crassa*, we found YPT-31 at the peripheral layer of the Spk surrounding the YPT-1 core (Fig. 6A). Given the distribution of both FM4–64 and YPT-31 at the peripheral layer of the Spk, we expected to obtain similar rates of recovery from bleaching for the fluorescent probe and the Rab protein. However, the $t_{1/2}$ of YPT-31 was significantly lower than the $t_{1/2}$ of FM4–64, suggesting that YPT-31 associates with a distinct subpopulation of macrovesicles at the Spk. An alternative explanation would be that FM4–64 labels membrane carriers that arrive at the Spk from a separate secretory route derived from endosomal recycling. Although additional biochemical approaches are needed to decipher the differential association of YPT-1 and YPT-31 with the vesicles of the Spk, the results of the localization experiments and the differences in $t_{1/2}$ indicate that the stratification of the Spk is delicately choreographed by Rab GTPases. Furthermore, we identified that SEC-4 distributed similarly to YPT-31 at the outer layer of the Spk (Fig. 6A). These results are consistent with the suggested role of Ypt31/32p and Sec4p in later traffic steps of the secretory pathway. Sec4 has been previously identified at hyphal tips of *C. albicans*, *Aspergillus fumigatus* and *Ashbya gossypii* (Schmitz *et al*., 2006; Jones and Sudbery, 2010; Powers-Fletcher *et al*., 2013). Notably, in *N. crassa*, not only SEC-4 but also YPT-31 is involved in the traffic of Spk macrovesicles. Recently, the characterization of the *N. crassa* exocyst complex revealed that subunits SEC-3, EXO-70 and EXO-84 partially associate with the outer macrovesicular layer of the Spk (Riquelme and Sánchez-León, 2014; Riquelme *et al*., 2014). In *C. albicans*, based on the differences in the dynamics and localization patterns observed for Sec4 and exocyst components Exo70 and Exo84, it has been proposed that secretory vesicles of the Spk associate with the exocyst at the cell surface (Jones and Sudbery, 2010). In *N. crassa*,

the partial co-localization of EXO-70 and YPT-31 at the Spk outer layer, suggests that the membrane carriers labeled by YPT-31 associate with the exocyst subunits (i.e. EXO-70) at the periphery of the Spk before being directed to exocytic sites. It remains to be tested whether any of these exocyst subunits serves as effectors of SEC-4 or YPT-31.

It is well recognized that the Golgi apparatus is an organelle that has a pivotal role in the secretory system of eukaryotic cells (Mowbrey and Dacks, 2009). In contrast to the stacked organization of the Golgi apparatus seen in some organisms, the fungal Golgi cisternae (early and late compartments) are scattered and optically resolvable by light microscopy (Wooding and Pelham, 1998). According to the proposed model for Golgi cisternal maturation, secretory cargoes are modified by a specific set of enzymes, which change over time within the same compartment (cisterna) (Losev *et al*., 2006; Matsuura-Tokita *et al*., 2006). This model assumes that the enzymes utilized in the early Golgi are recycled back from late Golgi through membrane carriers traveling in a retrograde manner; accordingly, a late Golgi cisterna corresponds to a mature early Golgi cisterna that has acquired 'late proteins'. Within the diverse fungal groups, there is wide evidence of variation in the organization and morphology of the Golgi apparatus. For instance, in contrast to the stacked cisternae of Golgi observed in *Schizosaccharomyces pombe* and *Pichia pastoris*, *S. cerevisiae*, *N. crassa* and *A. nidulans* have dispersed Golgi cisternae (Mogelsvang *et al*., 2003; Pantazopoulou and Peñalva, 2011; Bowman *et al*., 2012; Suda and Nakano, 2012; Pinar *et al*., 2013b). Protein secretion processes at Golgi require the orchestrated actions of distinct Rabs to ensure vesicle directionality to specific organelles (Hutagalung and Novick, 2011). The *S. cerevisiae* Ypt1p and the mammalian Rab1 have been implicated in the regulation of the traffic of vesicles from and to the distinct Golgi structures (Barrowman *et al*., 2010). In addition to the localization at hyphal tips, we identified YPT-1 at numerous punctate structures along the hyphae in *N. crassa*. The distribution pattern, pleomorphic nature and motility of these structures were similar to the structures previously labeled by various Golgi markers (Hubbard and Kaminskyj, 2008; Bowman *et al*., 2012; Pinar *et al*., 2013a). Our co-localization analysis of YPT-1 and putative early and late Golgi markers confirmed that this Rab GTPase associates with Golgi cisternae and participates in traffic events at the Golgi interface in *N. crassa*. A recent study in *A. nidulans* showed that BFA affects the morphology of the Golgi by promoting the aggregation of its cisternae (Pinar *et al*., 2013a). In *N. crassa*, exposure to BFA induced the formation of clusters of Golgi cisternae, which were labeled by GFP-YPT-1, but not with tDIMER-2-YPT-31, confirming that YPT-1 participates at the membrane trafficking events at the Golgi level. The lack of YPT-31 at similar structures and its exclusive localization at hyphal tips suggest that the *N. crassa* YPT-31 participates in post-Golgi steps of the secretory pathway, as previously shown for YPT-31/32 in the budding yeast (Jedd *et al*., 1997) and for RabE^{Rab11} in *A. nidulans* (Pantazopoulou *et al*., 2014). Under exposure to BFA, arrival of YPT-1 and YPT-31 to the Spk was only transiently blocked, while Golgi cisternae organization was disturbed. This suggests that YPT-1 and YPT-31 associated vesicles either reach the Spk by a Golgi-independent secretory pathway, as previously suggested for CHS (Riquelme *et al*., 2007), or alternatively, that the gradual recovery of Golgi cisternae from BFA effects allows some exit of secretory carriers destined to the Spk. Recently, the Ypt1p orthologue in *A. nidulans*, RabO^{Rab1}, was observed at distinct Golgi compartments identified as early and late Golgi cisternae, whose distribution varied in different regions of the hyphal apex (Pinar *et al*., 2013a). In *N. crassa*, YPT-1 and the early Golgi marker USO-1 partially co-localized within the same Golgi cisternae, although they occupied distinct regions, which reflects the progression of the Golgi cisternae during the distinct maturation stages. The asymmetrical distribution of the YPT-1/USO-1 labeled Golgi cisternae along the hyphae indicates the existence of a spatially organized secretory system that advances while at the same time keeps a certain distance from the apical zone. We also identified the putative early Golgi marker VRG-4 co-localizing with YPT-1 at some Golgi cisternae. Recently, in *C. albicans* Vrg4 was visualized at Golgi cisternae, which were predominantly localized at tip regions during hyphal formation (Rida *et al*., 2006). In *S. cerevisiae*, the GDP-mannose transporter encoded by *VRG4* has been identified at early Golgi cisternae (Abe *et al*., 2004; Losev *et al*., 2006). The average ICQ values in this case, namely VRG-4/YPT-1, were lower than those obtained for USO-1 and YPT-1. These differences between USO-1/YPT-1 and VRG-4/YPT-1 cisternae could be explained by the distinct residence time of each protein at the Golgi cisternae. While USO-1 could be required merely at tethering events at the early Golgi membranes (Beard *et al*., 2005), VRG-4 could reside at Golgi cisternae for longer periods, because it is needed for mannose transport (Jackson-Hayes *et al*., 2008). In *A. nidulans*, RabO^{Rab1} was found at late Golgi cisternae (Pinar *et al*., 2013a). Consistent with these observations, YPT-1 displayed some co-localization with the Golgi marker SEC-7, a prototypic late Golgi marker, in *N. crassa*, suggesting that a population of YPT-1 Golgi cisternae correspond to late Golgi. Partial co-localization of SEC-7 and VPS-52 was also found.

The lower average ICQ value obtained for YPT-1/SEC-7 in comparison with the ICQ value of YPT-1/VPS-52 might be explained by the fact that VPS-52 could also be at structures other than late Golgi cisternae. Although the human GARP complex is mainly associated with the TGN

(Perez-Victoria *et al*., 2008), it has also been detected at endosomal pools (Liewen *et al*., 2005). Except for VPS-52, exposure to BFA increased the co-localization between the different Golgi markers and YPT-1 at Golgi aggregates. In *A. nidulans*, by following the fate of fluorescently tagged PH^{OSBP}, it was shown that the late Golgi cisternae are transient structures that dissipate into $RabE^{Rab11}$ post-Golgi carriers (Pantazopoulou *et al*., 2014).

YPT-1 was also found decorating highly dynamic tubule-like structures at distal regions of the cells, which could correspond to the tubular endomembranes of the secretory system reported previously (Riquelme *et al*., 2007; Bowman *et al*., 2009; Sánchez-León *et al*., 2011). These tubular structures could be the fungal equivalents of the mammalian vesicular tubular clusters (VTCs) also referred to as ER-Golgi intermediate compartments or ERGICs (Sesso *et al*., 1994). Thus far, the existence of VTCs in fungal hyphae has not been explored. Further analyses are needed to identify the nature of the YPT-1 decorated tubules.

Various studies have shown that Rab GTPases play key roles in autophagy (Bento *et al*., 2013). Previously, it was identified that in *S. cerevisiae*, the TRAPPIII tethering complex acts as an autophagy-specific GEF for Ypt1p, which is essential for autophagy (Lynch-Day *et al*., 2010). The interaction of Ypt1p and its efector Atg11p, a scaffold protein required for autophagy, is required for assembly of the preautophagosomal structure (PAS) (Lipatova *et al*., 2012). Recently, it was demonstrated that autophagy in *A. nidulans* is dependent on $RabO^{Rab1}$ (Pinar *et al*., 2013b), which led to propose a homeostatic role between the Spk and autophagosomes (Pinar *et al*., 2013a). The putative relationship between the *N. crassa* YPT-1 and autophagosomes was beyond the scope of this work, and the role of the *N. crassa* YPT-1 in autophagy remains to be tested.

Rab5 is a small GTPase previously identified at early endosomes (Chavrier *et al*., 1990). The various roles attributed to this Rab include coordination of the uncoating of Clathrin-coated vesicles, cargo sequestration, and regulation of the fusion between endocytic membranes and microtubule based-motility of early endosomes (Stenmark *et al*., 1994; Nielsen *et al*., 1999; Rubino *et al*., 2000; Kümmel and Ungermann, 2014). Fungal orthologues of Rab5 have been identified at early endosomes and are involved in the endocytic membrane traffic pathway (Singer-Krüger *et al*., 1994; Abenza *et al*., 2010; Seidel *et al*., 2013). The yeast Ypt1p has a role at the late Golgi interface based on a screening of *ypt1* mutants blocked in the traffic from early endosome to late Golgi (Sclafani *et al*., 2010). In *N. crassa*, we found no co-localization between the early endosome marker YPT-52 (Seidel *et al*., 2013) and the structures labeled by YPT-1. Regardless of this lack of co-localization, we cannot rule out a role for YPT-1 in traffic steps between early endosomes and late Golgi. YPT-1 could be acting on the target membrane in endosome-to-Golgi traffic. Further mutant and biochemical analyses are needed to further understand their mode of operation.

Thus far, little is known about the relationship of Rab GTPases and the traffic of vesicles of the Spk. A better understanding on the role of Rab GTPases at late secretory traffic events would help to decipher the organizational differences found in the Spk of diverse filamentous fungal species.

Experimental procedures

Strains and culture conditions

Bacterial and *N. crassa* strains used or generated in this study are listed in Table S1. *Escherichia coli* DH5α was grown on LB medium (1% tryptone, 0.5% yeast extract, 1% NaCl) supplemented with ampicillin (100 μg ml^{-1}) and incubated at 37°C. *N. crassa* cells were routinely grown in Vogel's minimal medium (VMM) containing 1.5% sucrose and solidified with 1.5% agar when needed (Vogel, 1956). For auxotrophic His^- strains, histidine (0.5 mg ml^{-1}) was added to VMM medium. Transformed conidia were plated on VMM-FGS (0.5% fructose, 0.5% glucose, 20% sorbose) supplemented with hygromycin B (200 μm ml^{-1}; InvivoGen) when required. For crosses, *mat* a conidia were spread over *mat A* mycelium grown on solid synthetic crossing medium with 2% sucrose (Westergaard and Mitchel, 1947). For growth analysis, elongation rate of *N. crassa* transformants was measured on VMM agar plates at 30°C.

Recombinant DNA techniques and plasmid constructions

Plasmids and oligonucleotides used are described in Table S1. Standard polymerase chain reaction (PCR) and cloning procedures were used to fuse the *sgfp*, *mcherry* or *tdimer2* gene to the 5′ end of the ORFs of the Rab GTPases *ypt-1* (NCU08477.7), *ypt-31* (NCU01523.5), *sec-4* (NCU06404.7) or the vSNARE *syn-1* (NCU00566.7) in the plasmids PCCG::N-GFP (Honda and Selker, 2009), pJV18-N and pMF334 (Freitag and Selker, 2005) respectively. The open reading frames (ORFs) of *ypt-1* (1067 bp), *ypt-31* (837 bp), *sec-4* (959 bp) and *syn-1* (980 bp) were identified in *N. crassa* (www.broadinstitute.org/annotation/genome/neurospora/MultiHome.html) and amplified by PCR from *N. crassa* N1 (FGSC988) genomic DNA with custom-designed primers that included restriction endonucleases sites at the 5′ and 3′ termini. PCR was performed in a Bio-Rad Thermal Cycler using TaKaRa LA Taq® DNA polymerase (Clontech). PCR was performed with the following conditions: denaturation at 94°C (2 min) was followed by 30 cycles of 94°C (30 s), 55°C (30 s) and 72°C (2–2.5 min), and by a final extension at 72°C (5 min). For the s*gfp* gene fusion, the amplified and gel purified PCR products of the *ypt-1* and *sec-4* genes were digested with *Asc*I and *Xba*I and inserted into *Asc*I/*Xba*I-digested PCCG::N-GFP (GeneBank accession No. FJ457006) yielding plasmids

pESL07b-2 and pESL05b-2; while the PCR product of *syn-1* was digested with *Pac*I and *Xba*I, and inserted in PCCG::N-GFP plasmid digested with the same restriction endonucleases. For the *tdimer2* gene fusion, the amplified and gel purified PCR product of the *ypt-31* gene was digested with *Mlu*I and *Bgl*II and inserted into *Mlu*I/*Bgl*II-digested pMF334 (GeneBank accession No. DQ250999.1), yielding plasmid ptdimer2(12)-YPT-31. For the expression of *ypt-1* and *sec-4* under the control of their endogenous promoters, we amplified ~1 kb of the 5′ untranslated region of the corresponding ORFs, and inserted the PCR digested products into *Eco*RI/*Bam*HI digested pCoS204 (Seidel *et al*., 2013), replacing the *ccg-1* promoter (P*ccg-1*). Amplified and gel purified PCR ORFs of *ypt-1* and *sec-4* were *Pac*I/*Xba*I digested and subcloned in the corresponding promoter containing vectors.

To obtain *mcherry* gene fusions, the PCR products of *ypt-1* and *sec-4* were digested with *Pac*I and *Eco*RI and inserted into *Pac*I/*Eco*RI digested pJV18-N yielding plasmids pESL10-25 and pESL08-15 respectively. For the *sgfp* tagging of putative early and late Golgi markers, we searched the *N. crassa* genome sequences for orthologues of the *S. cerevisiae* coiled-coil tethering protein USO-1 (NCU01644.7) and SEC-7 (NCU07658.7), respectively, and designed primers to tag *uso-1* and *sec-7* endogenously at their C-terminus by using the split marker gene replacement method (Smith *et al*., 2011). The primers (Table S1) design and PCR strategy for the above technique were previously described (Riquelme and Sánchez-León, 2014; Riquelme *et al*., 2014). Additionally, we designed the primer pairs USO-1-F/USO-1-R-Gly and SEC-7-F-01/SEC-7-10xGLY-R to amplify ~1 kb fragments of the *uso-1* and *sec-7* ORFs, respectively, immediately upstream of the stop codon; while the primer pairs USO-1-UTR-F-lox/USO-1-UTR-R and LOX-3UTR-SEC-7-F/3UTR-SEC-7-R were designed to amplify ~1 kb fragments of the *uso-1* and *sec-7*, of their 3′ untranslated corresponding region. The resulting fused PCR fragments were gel purified, mixed in equal proportions (~0.5 μg DNA per transformation), and used to transform *N. crassa* NMF263 (FGSC9718) and/or N2928 (FGSC9717) conidia.

Neurospora genetics

Conidia of *N. crassa* host strains FGSC9717 or FGSC9718, deficient in nonhomologous end-joining (Ninomiya *et al*., 2004), were transformed with either *Nde*I or *Ssp*I linearized vectors or PCR products by electroporation in a Bio-Rad Gene Pulser (capacitance, 25 μF; voltage, 1.5 kV; resistance, 600 Ω) as previously described (Riquelme *et al*., 2007). For each transformation, 20 to 30 histidine prototrophs (His+) or hygromycin B (200 μg ml^{-1}) resistant (Hyg+) transformants were transferred to VMM slants and screened for the expression of GFP, mChFP or tDIMER-2 by confocal microscopy. Crossing of transformants was performed as previously described (Riquelme *et al*., 2007). To select homokaryons, the resulting ascospores were inoculated onto VMM plates, heat shocked at 60°C for 1 h and incubated at 25°C. No viable homokaryon knockout strains could be recovered for any of the Rabs analyzed, which hindered testing the functionality of any of the fluorescently tagged Rabs by complementation.

Blast search for *N. crassa* proteins SEC-4, YPT-31, SYN-1 and SEC-7 was performed using the GeneBank accession numbers XP_962242.1, XP_956972.2, XP_964727.2 and XP_962785.2 respectively (Altschul *et al*., 1990). Alignments of the Rab GTPases with their corresponding orthologues were performed in Geneious Basic 4.8.5 software (using the default program settings). Sequences of fungal and human Rabs identified with high level of identity were obtained using the GeneBank accession numbers listed in Table S2.

Microscopy analysis and image processing

Imaging of the transformant strains was conducted in three different confocal microscopes:

i. An inverted Zeiss LSM-510 Meta laser scanning confocal microscope (LSCM) fitted with an argon/2 ion laser (GFP: excitation, 488 nm; emission, 500 to 550 nm); For simultaneous visualization of GFP and mCherry an argon/2 and He/Ne-2 ion laser (mCherry: excitation 543–561 nm; emission, 575 to 615 nm) along with a 100× Ph3 Plan Neofluar oil-immersion objective (NA, 1.3) or 63× LCI Plan Neofluar Imm Korr DIC (NA, 1.3) were used for the confocal observations. Confocal images were captured using LSM-510 software (version 3.2; Carl Zeiss) and evaluated with a Carl Zeiss LSM Image Examiner software (version 4.2).

ii. An inverted Olympus Fluoview™ FV1000 confocal microscope fitted with an argon laser (GFP: excitation, 488 nm; emission, 505–525 nm) and a diode pump solid state (DPSS, Melles Griot, Carlsbad, CA) laser (mCherry or RFP: excitation, 543 nm; emission, 560–660 nm) was used for individual or sequential visualization of GFP and mCherry or tDIMER-2. A 60× Plan Apo N (Olympus) oil-immersion objective (NA, 1.42) was used with this equipment. Confocal images were captured and examined using FV10-ASW software (version 4.0.2.9, Olympus).

iii. An upright Leica DM5000 confocal microscope fitted with an argon laser (GFP: excitation, 488 nm; emission, 497–536 nm) and a DPSS laser (mCherry or tDIMER-2: excitation, 561 nm; emission, 568–646 nm) were used for individual or simultaneous visualizations of the fluorescent molecules. A 63× HCX PL APO lambda blue oil-immersion objective (NA, 1.4) was used. Confocal images were captured using TCS SP5 Leica System and examined using LAS AF software (version 2.6.3, Leica). For FRAP analysis, the fluorescent Spk of growing hyphae was photobleached for 5 s with the 488 nm argon laser or with 543 nm DPSS laser at ~ 50% of intensity, and fluorescence recovery images were captured at 0.61 to 3.39 s intervals at 2.5–5% of laser intensity. Fluorescence signal intensities of the Spk were analyzed with ImageJ (version 1.48u; Maryland, USA). Time series of images were converted to grayscale and the average pixel intensity of the Spk area was measured at every time point. Intensity values were normalized, considering the highest average intensity value after photobleaching as the 100%. Half-time recovery time ($t_{1/2}$, Mean ± Standard Error), i.e. the time at which half of the final fluorescence intensity was reached was calculated from the average of $t_{1/2}$ obtained from individual samples. For TIRFM, an IX-81 inverted microscope equipped with a 60× (NA, 1.49) Apo-N TIRF objective lens and DPSS lasers: 488 nm and 561 nm (Melles Griot, Carlsbad, CA), was used. Images were recorded with a Hamamatsu Digital Camera C11440 Orca-Flash 2.8 (Hamamatsu Photonics K.K., Japan) for durations of 2–3 min at 960 × 720

pixels resolution and 0.9 s per frame. Dimensions cell Sens software (version 1.9; Olympus Corporation) was used to control the camera and capture images. All images were further processed with Adobe Photoshop CS5 (version 15.0). Kymographs and the moving rates of YPT-1 fluorescent particles were obtained from TIRFM time series (70 frames in 64 s; 120.9 nm/pixel) using the Kymomaker software (Chiba *et al.*, 2014); the automatic trace detection function of the software was used to calculate the moving rates of individual particles that exhibited only short distance movements (~ 2.3 μm). One-way ANOVA, the post-hoc Tukey HSD test and Student's *t*-test statistical analysis were performed on the STATISTICA data analysis software system (version 8.0, StatSoft, Inc.). For time-lapse and live-cell imaging, the inverted agar block method was employed (Hickey *et al.*, 2005). For microscopy analyses of the hyphae under BFA treatment, a thin coverslip (0.17 μm, 22 × 22 mm) was placed between the microscope slide and the inverted agar block containing the growing hyphae (~ 0.5 mm away from the edge of the colony). After scanning untreated hyphae, the coverslip was subtly lifted to directly add 10 μl of BFA so we could immediately monitor the inhibitory effects over the same hyphae in less than 1 min. To analyze the *in vivo* co-localization of two proteins, heterokaryons were obtained on VMM agar plates, where conidia of two different *N. crassa* strains of the same mating type were co-inoculated and grown overnight at 28–30°C. For quantitative correlation image analysis of co-localization, the ICQ was assessed using ImageJ software (version 1.48u; Maryland, USA). Fluorescence intensities of the hyphal regions (~ 60 μm) analyzed were adjusted and the obtained values normalized.

Fluorescent dye and inhibitors

A stock solution (20 mg ml^{-1}) of the fungal metabolite brefeldin A (BFA; Sigma) was prepared in dimethyl sulfoxide and prepared fresh at a final concentration of 200–300 μg ml^{-1} in VMM. For staining of the endocytic membranes, we used 10–25 μM of the styryl dye FM4–64 (N-(3-triethylammoniumpropyl)-4-(6-(4-(diethylamino)phenyl)hexatrienyl) pyridinium dibromide) (Molecular Probes®). For each dye or inhibitor, the agar blocks containing hyphae were inverted onto coverslips containing 5 to 10 μl of the diluted working stock.

Density gradient centrifugation and Western blots

Conidia (1×10^4 cells ml^{-1}) from the selected transformed strains were inoculated into 200–500 ml Vogel's complete medium (VCM) and incubated at 30°C, under 220 r.p.m. agitation, for 20 h. Mycelia were harvested by filtration, washed twice with sterile cold deionized water, and once with homogenization buffer (33 mM phosphate buffer, pH 8.2). Mycelia (~10 g) were mixed with 10 ml homogenization buffer (33 mM, pH 8.2), protease inhibitors, 20 g of glass beads (425–600 microns, Sigma), and were disrupted at a low temperature in a Braun MSK homogenizer for 4 × 30 s. Disrupted cells were centrifuged at 1000 × *g* (R_{av}) at 4°C for 10 min, and the supernatant was layered on top of a 35 ml linear sucrose gradient (10–65%, w/v) in homogenization buffer. The mix was centrifuged at 184 000 × *g* (R_{av}) for 4 h, at 4°C in a Beckman ultracentrifuge using a 70Ti rotor. The gradient was fractionated from the top with an ISCO fractionator using 70% (w/v) sucrose as chasing solution. Fifty to 100 μl of each fraction were mixed with Laemmli buffer (2×), boiled for 5 min and kept at –20°C until their analysis by Western blot. For expression analysis of the GFP-YPT-1 constructs driven by the P*ccg-1* and P*ypt-1* promoters, fresh conidia from the corresponding strains were grown in Vogel's liquid medium at 30°C and 150 r.p.m. for ~20 h. Mycelia were harvested by filtration, washed twice with sterile cold deionized water, and pulverized with liquid nitrogen. Pulverized mycelia (5–8 ml) were mixed with 25 ml of lysis buffer (Tris-HCl 50 mM, pH 7.4; KCl 100 mM; $MgCl_2$ 10 mM; Triton X-100 1%) and protease inhibitors. Disrupted cells were centrifuged at 2850 × *g* (R_{max}) at 4°C for 25 min, and the supernatant was centrifuged at 19 000 × *g* at 4°C for 1 h. Two hundred microliters of the supernatant of each sample was mixed with Laemmli buffer (2×), boiled for 5 min and kept at –20°C until their analysis by Western blot.

For Western blot analysis, 30 μl of the selected fractions or 40 μg of total protein equivalent as bovine serum albumin (BSA) were separated by 8–13.5% SDS-PAGE. Resolved proteins were transferred to Nitrocellulose (Pall Corporation) or PVDF (Millipore) filter membranes, which were immunoreacted for GFP- or mChFP-tagged proteins with a mouse anti-GFP antibody 1:1000 (Santa Cruz Biotechnology, SC-9996), rabbit polyclonal mChFP antibody 1:1000 (Gene Tex, GTX59788) or mouse anti-β-actin antibody 1:1000 (Abcam, 20272) respectively. Membranes were revealed with a peroxidase-conjugated anti-mouse antibody 1:3000 (Roche, 04719930001) or anti-rabbit antibody 1:25 000 (Sigma, A0545) and Pierce enhanced chemiluminescent assays. Densitometry of the Western blot bands was analyzed with ImageJ Software (version 1.48u; Maryland, USA).

Acknowledgements

We thank Dr. Robert W. Roberson (Arizona State University, Tempe, AZ) and Dr. Alfredo Herrera-Estrella (National Laboratory of Genomics for Biodiversity, CINVESTAV, Irapuato-México) for kindly letting us use their Zeiss Confocal Microscopy equipment while ours was out of service. We appreciate I.B.Q. Pedro Martínez-Hernández for technical assistance. We are indebted to the Fungal Genetics Stock Center and the Neurospora Functional Genomics Program Project for materials and strains. We are grateful to Dr. Michael Freitag for hosting M.R. to conduct the USO-1 endogenous tagging and to M.Sc. Adriana Romero Olivares for generating USO-1-GFP homokaryon strain and the VMRP-74 vector. We give special thanks to Dr. Salomón Bartnicki-García for his valuable contribution to discussions and commentaries to this work. This work was financially supported by the Consejo Nacional de Ciencia y Tecnología, CONACYT grants: CB-2008-105-600-Q, I0010-2001-01, and CONACYT-DFG I0110/193/10 FON.INST.-30-10 to M.R. and grants 290604 and 290673 to E.S-L.

References

Abe, M., Noda, Y., Adachi, H., and Yoda, K. (2004) Localization of GDP-mannose transporter in the Golgi requires

retrieval to the endoplasmic reticulum depending on its cytoplasmic tail and coatomer. *J Cell Sci* **117:** 5687–5696.
Abenza, J.F., Galindo, A., Pantazopoulou, A., Gil, C., de los Rios, V., and Peñalva, M.A. (2010) *Aspergillus* RabB^{Rab5} integrates acquisition of degradative identity with the long distance movement of early endosomes. *Mol Biol Cell* **21:** 2756–2769.
Achstetter, T., Franzusoff, A., Field, C., and Schekman, R. (1988) SEC7 encodes an unusual, high molecular weight protein required for membrane traffic from the yeast Golgi apparatus. *J Biol Chem* **263:** 11711–11717.
Allan, B.B., Moyer, B., and Balch, W.E. (2000) Rab1 Recruitment of p115 into a cis-SNARE complex: programming budding COPII vesicles for Fusion. *Science* **289:** 444–448.
Altschul, S.F., Gish, W., Miller, W., Myers, E.W., and Lipman, D.J. (1990) Basic local alignment search tool. *J Mol Biol* **215:** 403–410.
Barr, F., Nakamura, N., and Warren, G. (1998) Mapping the interaction between GRASP65 and GM130, components of a protein complex involved in the stacking of Golgi cisternae. *EMBO J* **17:** 3258–3268.
Barrowman, J., Bhandari, D., Reinisch, K., and Ferro-Novick, S. (2010) TRAPP complexes in membrane traffic: convergence through a common Rab. *Nat Rev Mol Cell Biol* **11:** 759–763.
Bartnicki-Garcia, S. (1990) Role of vesicles in apical growth and a new mathematical model of hyphal morphogenesis. In *Tip Growth in Plant and Fungal Cells*. Heath, I.B. (ed.). San Diego, CA: Academic Press, pp. 211–232.
Bartnicki-Garcia, S., Bracker, C.E., Lippman, E., and Ruiz-Herrera, J. (1984) Chitosomes from the wall-less 'slime' mutant of *Neurospora crassa*. *Arch Microbiol* **139:** 105–112.
Bartnicki-Garcia, S., Hergert, F., and Gierz, G. (1989) Computer simulation of fungal morphogenesis and the mathematical basis for hyphal (tip) growth. *Protoplasma* **153:** 46–57.
Beard, M., Satoh, A., Shorter, J., and Warren, G. (2005) A cryptic Rab1-binding site in the p115 tethering protein. *J Biol Chem* **280:** 25840–25848.
Benli, M., Doring, F., Robinson, D.G., Yang, X., and Gallwitz, D. (1996) Two GTPase isoforms, Ypt31p and Ypt32p, are essential for Golgi function in yeast. *EMBO J* **15:** 6460–6475.
Bento, C.F., Puri, C., Moreau, K., and Rubinsztein, D.C. (2013) The role of membrane-trafficking small GTPases in the regulation of autophagy. *J Cell Sci* **126:** 1059–1069.
Borkovich, K.A., Alex, L.A., Yarden, O., Freitag, M., Turner, G.E., Read, N.D., *et al*. (2004) Lessons from the genome sequence of *Neurospora crassa*: tracing the path from genomic blueprint to multicellular organism. *Microbiol Mol Biol Rev* **68:** 1–108.
Bourett, T.M., James, S.W., and Howard, R.J. (2007) The endomembrane system of the fungal cell. In *Biology of the Fungal Cell*. Howard, R.J., and Gow, N.A.R. (eds). Berlin, Heidelberg: Springer-Verlag, pp. 1–47.
Bowman, B.J., Draskovic, M., Freitag, M., and Bowman, E.J. (2009) Structure and distribution of organelles and cellular location of calcium transporters in *Neurospora crassa*. *Eukaryot Cell* **8:** 1845–1855.
Bowman, B.J., Abreu, S., Johl, J.K., and Bowman, E.J. (2012) The *pmr* gene, encoding a Ca^{2+}-ATPase, is required for calcium and manganese homeostasis and normal development of hyphae and conidia in *Neurospora crassa*. *Eukaryot Cell* **11:** 1362–1370.
Cao, X., Ballwe, N., and Barlowe, C. (1998) Initial docking of ER-derived vesicles requires Uso1p and Ypt1p but is independent of SNARE proteins. *EMBO J* **17:** 2156–2165.
Chavrier, P., Parton, R.G., Hauri, H.P., Simons, K., and Zerial, M. (1990) Localization of low molecular weight GTP binding proteins to exocytic and endocytic compartments. *Cell* **62:** 317–329.
Chiba, K., Shimada, Y., Kinjo, M., Suzuki, T., and Uchida, S. (2014) Simple and direct assembly of kymographs from movies using KYMOMAKER. *Traffic* **15:** 1–11.
Conibear, E., and Stevens, T.H. (2000) Vps52p, Vps53p, and Vps54p form a novel multisubunit complex required for protein sorting at the yeast late Golgi. *Mol Biol Cell* **11:** 306–323.
Dean, N., Zhang, Y.B., and Poster, J.B. (1997) The VRG4 gene is required for GDP-mannose transport into the lumen of the golgi in the yeast, *Saccharomyces cerevisiae*. *J Biol Chem* **272:** 31908–31914.
Dijksterhuis, J., and Molenaar, D. (2013) Vesicle trafficking via the Spitzenkörper during hyphal tip growth in *Rhizoctonia solani*. *Antonie Van Leeuwenhoek* **103:** 921–931.
Du, L.-L., and Novick, P. (2001) Yeast Rab GTPase-activating Protein Gyp1p localizes to the golgi apparatus and is a negative regulator of Ypt1p. *Mol Biol Cell* **12:** 1215–1226.
Faso, C., Boulaflous, A., and Brandizzi, F. (2009) The plant Golgi apparatus: last 10 years of answered and open questions. *FEBS Lett* **583:** 3752–3757.
Fischer-Parton, S., Parton, R.M., Hickey, P.C., Dijksterhuis, J., Atkinson, H.A., and Read, N.D. (2000) Confocal microscopy of FM4–64 as a tool for analysing endocytosis and vesicle trafficking in living fungal hyphae. *J Microsc* **198:** 246–259.
Freitag, M., and Selker, E.U. (2005) Expression and visualization of red fluorescent protein (RFP) in *Neurospora crassa*. *Fungal Genet Newsl* **52:** 14.
Geitmann, A., and Emons, A.M. (2000) The cytoskeleton in plant and fungal cell tip growth. *J Microsc* **198:** 218–245.
Girbardt, M. (1970) Die ultrastruktur der apikalregion von pilzhyphen. *Protoplasma* **67:** 413–441.
Goud, B., Salminen, A., Walworth, N.C., and Novick, P. (1988) A GTP-binding protein required for secretion rapidly associates with secretory vesicles and the plasma membrane in yeast. *Cell* **53:** 753–768.
Grosshans, B.L., Ortiz, D., and Novick, P. (2006) Rabs and their effectors: achieving specificity in membrane traffic. *Proc Natl Acad Sci USA* **103:** 11821–11827.
Grote, E., Carr, C.M., and Novick, P.J. (2000) Ordering the final events in yeast exocytosis. *J Cell Biol* **151:** 439–452.
Grove, S., and Bracker, C.E. (1970) Protoplasmic organization of hyphal tips among fungi: vesicles and Spitzenkörper. *J Bacteriol* **104:** 989–1009.
Guo, W., Roth, D., Walch-Solimena, C., and Novick, P. (1999) The exocyst is an effector for Sec4p, targeting secretory vesicles to sites of exocytosis. *EMBO J* **18:** 1071–1088.
Heath, I.B. (1990) The roles of actin in tip growth of fungi. *Int Rev Cytol* **123:** 95–127.
Heintz, K., Palme, K., Diefenthal, T., and Russo, V.E. (1992)

The *Ncypt1* gene from *Neurospora crassa* is located on chromosome 2: molecular cloning and structural analysis. *Mol Gen Genet* **235:** 413–421.
Hickey, P.C., Jacobson, D.J., Read, N.D., and Glass, N.L. (2002) Live-cell imaging of vegetative hyphal fusion in *Neurospora crassa*. *Fungal Genet Biol* **37:** 109–119.
Hickey, P.C., Swift, S.R., Roca, M.G., and Read, N.D. (2005) Live-cell imaging of filamentous fungi using vital fluorescent dyes and confocal microscopy. *Methods Microbiol* **34:** 63–87.
Honda, S., and Selker, E.U. (2009) Tools for fungal proteomics: multifunctional *Neurospora* vectors for gene replacement, protein expression and protein purification. *Genetics* **182:** 11–23.
Horio, T., and Oakley, B.R. (2005) The role of microtubules in rapid hyphal tip growth of *Aspergillus nidulans*. *Mol Biol Cell* **16:** 918–926.
Howard, R. (1981) Ultrastructural analysis of hyphal tip cell growth in fungi: Spitzenkörper, cytoskeleton and endomembranes after freeze-substitution. *J Cell Sci* **48:** 89–103.
Hubbard, M.A., and Kaminskyj, S.G. (2008) Rapid tip-directed movement of golgi equivalents in growing *Aspergillus nidulans* hyphae suggests a mechanism for delivery of growth-related materials. *Microbiology* **154:** 1544–1553.
Hutagalung, A., and Novick, P. (2011) Role of Rab GTPases in membrane traffic and cell physiology. *Physiol Rev* **91:** 119–149.
Jackson-Hayes, L., Hill, T.W., Loprete, D.M., Fay, L.M., Gordon, B.S., Nkashama, S.A., *et al*. (2008) Two GDP-mannose transporters contribute to hyphal form and cell wall integrity in *Aspergillus nidulans*. *Microbiology* **154:** 2037–2047.
Jedd, G., Mulholland, J., and Segev, N. (1997) Two new Ypt GTPases are required for exit from the yeast *trans*-golgi compartment. *J Cell Biol* **137:** 563–580.
Jones, L.A., and Sudbery, P.E. (2010) Spitzenkörper, exocyst, and polarisome components in *Candida albicans* hyphae show different patterns of localization and have distinct dynamic properties. *Eukaryot Cell* **9:** 1455–1465.
Kümmel, D., and Ungermann, C. (2014) Principles of membrane tethering and fusion in endosome and lysosome biogenesis. *Curr Opin Cell Biol* **29:** 61–66.
Lafourcade, C., Galan, J.M., Gloor, Y., Haguenauer-Tsapis, R., and Peter, M. (2004) The GTPase-Activating enzyme Gyp1p is required for recycling of internalized membrane material by inactivationof the Rab/Ypt GTPase Ypt1p. *Mol Cell Biol* **24:** 3815–3826.
Leal-Morales, C.A., Bracker, C.E., and Bartnicki-Garcia, S. (1994) Distribution of chitin synthetase and various membrane marker enzymes in chitosomes and other organelles of the slime mutant of *Neurospora crassa*. *Exp Mycol* **18:** 168–179.
Lewis, M.J., Nichols, B.J., Prescianotto-Baschong, C., Riezman, H., and Pelham, H.R. (2000) Specific retrieval of the exocytic SNARE Snc1p from early yeast endosomes. *Mol Biol Cell* **11:** 23–38.
Li, Q., Lau, A., Morris, T.J., Guo, L., Fordyce, C.B., and Stanley, E.F. (2004) A syntaxin 1, $G\alpha_o$, and N-type calcium channel complex at a presynaptic nerve terminal: analysis by quantitative immunocolocalization. *J Neurosci* **24:** 4070–4081.
Liewen, H., Meinhold-Heerlein, I., Oliveira, V., Schwarzenbacher, R., Luo, G., Wadle, A., *et al*. (2005) Characterization of the human GARP (Golgi associated retrograde protein) complex. *Exp Cell Res* **306:** 24–34.
Lipatova, Z., Belogortseva, N., Zhang, X.Q., Kim, J., Taussig, D., and Segev, N. (2012) Regulation of selective autophagy onset by a Ypt/Rab GTPase module. *Proc Natl Acad Sci USA* **109:** 6981–6986.
Liu, S., and Storrie, B. (2012) Are Rab proteins the link between Golgi organization and membrane trafficking? *Cell Mol Life Sci* **69:** 4093–4106.
Losev, E., Reinke, C.A., Jellen, J., Strongin, D.E., Bevis, B.J., and Glick, B.S. (2006) Golgi maturation visualized in living yeast. *Nature* **441:** 1002–1006.
Lowe, M. (2011) Structural organization of the golgi apparatus. *Curr Opin Cell Biol* **23:** 85–93.
Lynch-Day, M.A., Bhandari, D., Menon, S., Huang, J., Cai, H., Bartholomew, C.R., *et al*. (2010) Trs85 directs a Ypt1 GEF, TRAPPIII, to the phagophore to promote autophagy. *Proc Natl Acad Sci USA* **107:** 7811–7816.
McNally, M.T., and Free, S.J. (1988) Isolation and characterization of a Neurospora glucose-repressible gene. *Curr Genet* **14:** 545–551.
Matsuura-Tokita, K., Takeuchi, M., Ichihara, A., Mikuriya, K., and Nakano, A. (2006) Live imaging of yeast Golgi cisternal maturation. *Nature* **441:** 1007–1010.
Mizuno-Yamasaki, E., Rivera-Molina, F., and Novick, P. (2012) GTPase networks in membrane traffic. *Annu Rev Biochem* **81:** 637–659.
Mogelsvang, S., Gomez-Ospina, N., Soderholm, J., Glick, B.S., and Staehelin, L.A. (2003) Tomographic evidence for continuous turnover of golgi cisternae in *Pichia pastoris*. *Mol Biol Cell* **14:** 2277–2291.
Mowbrey, K., and Dacks, J.B. (2009) Evolution and diversity of the golgi body. *FEBS Lett* **583:** 3738–3745.
Moyer, B., Allan, B.B., and Balch, W.E. (2001) Rab1 interaction with a GM130 effector complex regulates COPII vesicle cis-golgi tethering. *Traffic* **2:** 268–276.
Mukhopadhyay, A., Nieves, E., Che, F.-Y., Wang, J., Jin, L., Murray, J.W., *et al*. (2011) Proteomic analysis of endocytic vesicles: Rab1a regulates motility of early endocytic vesicles. *J Cell Sci* **124:** 765–775.
Nielsen, E., Severin, F., Backer, J.M., Hyman, A.A., and Zerial, M. (1999) Rab5 regulates motility of early endosomes on microtubules. *Nat Cell Biol* **1:** 376–382.
Ninomiya, Y., Suzuki, K., Ishii, C., and Inoue, H. (2004) Highly efficient gene replacements in *Neurospora* strains deficient for nonhomologous end-joining. *Proc Natl Acad Sci USA* **101:** 12248–12253.
Nishikawa, A., Poster, J.B., Jigami, Y., and Dean, N. (2002) Molecular and phenotypic analysis of CaVRG4, encoding an essential golgi apparatus GDP-mannose transporter. *J Bacteriol* **184:** 29–42.
Noda, Y., and Yoda, K. (2013) Molecular mechanisms of the localization of membrane proteins in the yeast golgi compartments. *Biosci Biotechnol Biochem* **77:** 435–445.
Ortiz, D., Medkova, M., Walch-Solimena, C., and Novick, P. (2002) Ypt32 recruits the Sec4p guanine nucleotide

exchange factor, Sec2p, to secretory vesicles; evidence for a Rab cascade in yeast. *J Cell Biol* **157:** 1005–1015.
Pantazopoulou, A., and Peñalva, M.A. (2009) Organization and dynamics of the *Aspergillus nidulans* golgi during apical extension and mitosis. *Mol Biol Cell* **20:** 4335–4347.
Pantazopoulou, A., and Peñalva, M.A. (2011) Characterization of *Aspergillus nidulans* RabC/Rab6. *Traffic* **12:** 386–406.
Pantazopoulou, A., Pinar, M., Xiang, X., and Penalva, M.A. (2014) Maturation of late Golgi cisternae into RabE^{RAB11} exocytic post-Golgi carriers visualized in vivo. *Mol Biol Cell* **25:** 2428–2443.
Pereira-Leal, J.B., and Seabra, M.C. (2000) The mammalian Rab family of small GTPases: definition of family and subfamily sequence motifs suggests a mechanism for functional specificity in the Ras superfamily. *J Mol Biol* **301:** 1077–1087.
Perez-Victoria, F.J., Mardones, G.A., and Bonifacino, J.S. (2008) Requirement of the human GARP complex for mannose 6-phosphate-receptor-dependent sorting of cathepsin D to lysosomes. *Mol Biol Cell* **19:** 2350–2362.
Pinar, M., Pantazopoulou, A., Arst, H.N., Jr, and Peñalva, M.A. (2013a) Acute inactivation of the *Aspergillus nidulans* golgi membrane fusion machinery: correlation of apical extension arrest and tip swelling with cisternal disorganization. *Mol Microbiol* **89:** 228–248.
Pinar, M., Pantazopoulou, A., and Penalva, M.A. (2013b) Live-cell imaging of Aspergillus nidulans autophagy: RAB1 dependence, Golgi independence and ER involvement. *Autophagy* **9:** 1024–1043.
Powers-Fletcher, M.V., Feng, X., Krishnan, K., and Askew, D.S. (2013) Deletion of the *sec4* homolog *srgA* from *Aspergillus fumigatus* is associated with an impaired stress response, attenuated virulence and phenotypic heterogeneity. *PLoS ONE* **8:** e66741.
Protopopov, V., Govindan, B., Novick, P., and Gerst, J.E. (1993) Homologs of the synaptobrevin/VAMP family of synaptic vesicle proteins function on the late secretory pathway in *S. cerevisiae*. *Cell* **74:** 855–861.
Rida, P.C., Nishikawa, A., Won, G.Y., and Dean, N. (2006) Yeast-to-hyphal transition triggers formin-dependent Golgi localization to the growing tip in *Candida albicans*. *Mol Biol Cell* **17:** 4364–4378.
Riquelme, M., and Sánchez-León, E. (2014) The spitzenkörper: a choreographer of fungal growth and morphogenesis. *Curr Opin Cell Biol* **20:** 27–33.
Riquelme, M., Bartnicki-García, S., González-Prieto, J.M., Sánchez-León, E., Verdín-Ramos, J.A., Beltrán-Aguilar, A., and Freitag, M. (2007) Spitzenkörper localization and intracellular traffic of green fluorescent protein-labeled CHS-3 and CHS-6 chitin synthases in living hyphae of *Neurospora crassa*. *Eukaryot Cell* **6:** 1853–1864.
Riquelme, M., Yarden, O., Bartnicki-García, S., Bowman, B., Castro-Longoria, E., Free, S.J., *et al*. (2011) Architecture and development of the *Neurospora crassa* hypha – a model cell for polarized growth. *Fungal Biol* **115:** 446–474.
Riquelme, M., Bredeweg, E.L., Callejas-Negrete, O., Roberson, R.W., Ludwig, S., Beltran-Aguilar, A., *et al*. (2014) The *Neurospora crassa* exocyst complex tethers Spitzenkörper vesicles to the apical plasma membrane during polarized growth. *Mol Biol Cell* **25:** 1312–1326.
Roberson, R.W., and Vargas, M.M. (1994) The tubulin cytoskeleton and its sites of nucleation in hyphal tips of *Allomyces macrogynus*. *Protoplasma* **182:** 19–31.
Rubino, M., Miaczynska, M., Lippé, R., and Zerial, M. (2000) Selective membrane recruitment of EEA1 suggests a role in directional transport of clathrin-coated vesicles to early endosomes. *J Biol Chem* **275:** 3745–3748.
Sánchez-León, E., Verdín, J., Freitag, M., Roberson, R.W., Bartnicki-Garcia, S., and Riquelme, M. (2011) Traffic of chitin synthase 1 (CHS-1) to the Spitzenkörper and developing septa in hyphae of *Neurospora crassa*: actin dependence and evidence of distinct microvesicle populations. *Eukaryot Cell* **10:** 683–695.
Sacher, M., Barrowman, J., Wang, W., Horecka, J., Zhang, Y., Pypaert, M., and Ferro-Novick, S. (2001) TRAPP I implicated in the specificity of tethering in ER-to-golgi transport. *Mol Cell* **7:** 433–442.
Salminen, A., and Novick, P. (1987) A ras-like protein is required for a post-golgi event in yeast secretion. *Cell* **49:** 527–538.
Sata, M., Donaldson, J.G., Moss, J., and Vaughan, M. (1998) Brefeldin A-inhibited guanine nucleotide-exchange activity of Sec7 domain from yeast Sec7 with yeast and mammalian ADP ribosylation factors. *Proc Natl Acad Sci USA* **95:** 4204–4208.
Schmitz, H.P., Kaufmann, A., Kohli, M., Laissue, P.P., and Philippsen, P. (2006) From function to shape: a novel role of a formin in morphogenesis of the fungus *Ashbya gossypii*. *Mol Biol Cell* **17:** 130–145.
Schultz, J., Doerks, T., Ponting, C.P., Copley, R.R., and Bork, P. (2000) More than 1000 putative new human signalling proteins revealed by EST data mining. *Nat Genet* **25:** 201–204.
Sclafani, A., Chen, S., Rivera-Molina, F., Reinisch, K., Novick, P., and Ferro-Novick, S. (2010) Establishing a role for the GTPase Ypt1p at the late golgi. *Traffic* **11:** 520–532.
Seidel, C., Moreno-Velásquez, S.D., Riquelme, M., and Fischer, R. (2013) *Neurospora crassa* NKIN2, a kinesin-3 motor, transports early endosomes and is required for polarized growth. *Eukaryot Cell* **12:** 1020–1032.
Sesso, A., de Faria, F.P., Iwamura, E.S., and Correa, H. (1994) A three-dimensional reconstruction study of the rough ER-Golgi interface in serial thin sections of the pancreatic acinar cell of the rat. *J Cell Sci* **107** (Part 3): 517–528.
Shanks, S.G., Carpp, L.N., Struthers, M.S., McCann, R.K., and Bryant, N.J. (2012) The Sec1/Munc18 protein Vps45 regulates cellular levels of its SNARE binding partners Tlg2 and Snc2 in *Saccharomyces cerevisiae*. *PLoS ONE* **7:** e49628.
Shorter, J., and Warren, G. (1999) A role for the vesicle tethering protein, p115, in the post-mitotic stacking of reassembling Golgi cisternae in a cell-free system. *J Cell Biol* **146:** 57–70.
Singer-Krüger, B., Stenmark, H., Düsterhöft, A., Philippsen, P., Yoo, J.-S., Gallwitz, D., and Zerial, M. (1994) Role of three Rab5-like GTPases, Ypt51p, Ypt52p, and Ypt53p, in the endocytic and vacuolar protein sorting pathways of yeast. *J Cell Biol* **125:** 283–298.
Siniossoglou, S., and Pelham, H.R. (2001) An effector os Ypt6p binds the SNARE Tlg1p and mediates selective

fusion of vesicles with late golgi membranes. *EMBO J* **20:** 5991–5998.
Smith, K.M., Phatale, P.A., Sullivan, C.M., Pomraning, K.R., and Freitag, M. (2011) Heterochromatin is required for normal distribution of *Neurospora crassa* CenH3. *Mol Cell Biol* **31:** 2528–2542.
Stenmark, H., Parton, R.G., Steele-Mortimer, O., Lütcke, A., Gruenberg, J., and Zerial, M. (1994) Inhibition of rab5 GTPase activity stimulates membrane fusion in endocytosis. *EMBO J* **13:** 1287–1296.
Suda, Y., and Nakano, A. (2012) The yeast Golgi apparatus. *Traffic* **13:** 505–510.
Suvorova, E.S., Duden, R., and Lupashin, V.V. (2002) The Sec34/Sec35p complex, a Ypt1p effector required for retrograde intra-Golgi trafficking, interacts with Golgi SNAREs and COPI vesicle coat proteins. *J Cell Biol* **157:** 631–643.
Taheri-Talesh, N., Horio, T., Araujo-Bazan, L., Dou, X., Espeso, E.A., Peñalva, M.A., *et al.* (2008) The tip growth apparatus of *Aspergillus nidulans*. *Mol Biol Cell* **19:** 1439–1449.
Verdín, J., Bartnicki-Garcia, S., and Riquelme, M. (2009) Functional stratification of the spitzenkörper of *Neurospora crassa*. *Mol Microbiol* **74:** 1044–1053.
Vogel, H.J. (1956) A convenient growth medium for *Neurospora* (medium N). *Microbiol Genet Bull* **13:** 42–43.
Westergaard, M., and Mitchel, H.K. (1947) *Neurospora* V. A synthetic medium favoring sexual reproduction. *Am J Bot* **14:** 573–577.
Wooding, S., and Pelham, H.R. (1998) The dynamics of golgi protein traffic visualized in living yeast cells. *Mol Biol Cell* **9:** 2667–2680.

Supporting information

Additional supporting information may be found in the online version of this article at the publisher's web-site.